

A Radio Continuum Survey of the Galactic Plane at 10 GHz

Toshihiro HANNA, Yoshiaki SOFUE,* Naomasa NAKAI,
Hisashi HIRABAYASHI, and Makoto INOUE

*Nobeyama Radio Observatory,[†]
Minamimaki-mura, Minamisaku-gun, Nagano 384-13*

(Received 1986 December 22; accepted 1987 July 24)

Abstract

A 10-GHz radio continuum survey of the galactic plane in the range $355^\circ \leq l \leq 56^\circ$, $-1^\circ 5 \leq b \leq +1^\circ 5$ was made at the Nobeyama Radio Observatory using the 45-m telescope. The half-power beam size of the resultant map is $3' 0$ and the noise level of the resultant map is typically 15 mK in brightness temperature. Thirty-one contour maps and a list of 144 small-diameter sources are presented.

Key words: Galactic structure; Radio continuum survey; Radio sources; The Galaxy.

1. Introduction

The radio continuum emission from the Galaxy is mainly composed of the synchrotron emission radiated by the interaction between relativistic electrons and the galactic magnetic field, and of the thermal emission by free-free transitions in ionized (H II) gases. These two types of emission can be separated by their spectra. At higher frequency the synchrotron emission from the galactic plane becomes weak, and we can easily recognize the weak and/or distant H II regions, Crablike supernova remnants, inverted spectrum sources, and diffuse thermal emission. The turnover frequency of the galactic background emission from nonthermal to thermal is about 3 GHz, and at 15.5 GHz about 70% to 90% of the radiation is of thermal origin (Hirabayashi 1974).

A number of continuum surveys have been made so far at various frequencies to investigate the galactic diffuse emission and discrete sources [for example, Altenhoff et al. (1970) at 1.4, 2.7, and 5 GHz, Day et al. (1972) at 2.7 GHz, Reich et al. (1984) at 2.7 GHz, Altenhoff et al. (1979) at 4.9 GHz, Haynes et al. (1978) at 5 GHz]. Among them the Effelsberg 4.875-GHz survey (Altenhoff et al. 1979) was made at the highest frequency with the sharpest beam ($2' 6$). However, it is difficult to separate

* Also of the Department of Astronomy, Faculty of Science, University of Tokyo, Bunkyo-ku, Tokyo 113.

[†] Nobeyama Radio Observatory, a branch of the Tokyo Astronomical Observatory, University of Tokyo, is a facility open for general use by researchers in the field of astronomy, astrophysics, and astrochemistry.

thermal and nonthermal components using previous surveys.

To investigate the galactic thermal emission and flat/inverted spectrum objects, we conducted a survey of the galactic plane at 10 GHz using the 45-m telescope at the Nobeyama Radio Observatory (NRO). A part of this survey ($21^\circ \leq l \leq 26^\circ$, $-1^\circ \leq b \leq +1^\circ$) has been already published (Sofue et al. 1984), in which a Crablike supernova remnant, two H II rings, and weak nonthermal sources were found.

This paper presents the main part of the survey work covering the narrow galactic ridge region of $356^\circ \leq l \leq 56^\circ$, $-1^\circ 5 \leq b \leq +1^\circ 5$.

2. Observations

The observations were made in March, April, and June 1983, in May, June, August, September, and December 1984, in June 1985, and in June 1986. It took 26 fine weather days to complete the observations and the total observing time with useful data was about 105 hr. The center frequency was 10.05 GHz in March and April 1983, and 10.55 GHz in June 1983 to September 1984. The instantaneous bandwidth was 500 MHz in both periods. Since September 1984, a multichannel backend, which can acquire radio continuum data at some different frequencies simultaneously, was available. We used a two-channel mode with center frequencies of 10.05 and 10.55 GHz. The instantaneous bandwidth was 500 MHz for either channel. As a result, almost the whole area of the survey was observed at 10.55 GHz except the

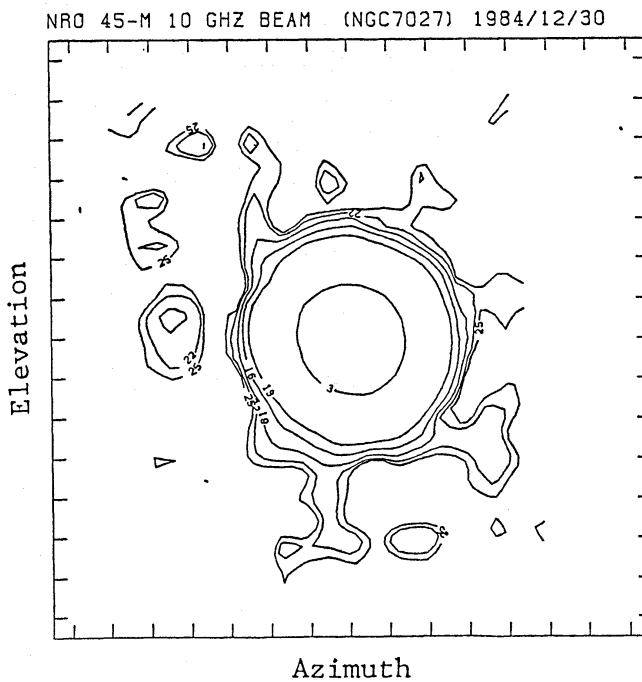


Fig. 1. Antenna beam pattern (point response pattern) at 10 GHz of the NRO 45-m telescope. Horizontal and vertical directions correspond to azimuthal and elevational directions, respectively. The pattern could be well approximated by a Gaussian pattern. The side-lobe level was less than -16 dB of the peak intensity. The contour levels are -3 , -13 , -16 , -19 , -22 , and -25 dB with respect to the peak intensity. The tick marks along the frame of the map are separated by $1'$.

Table 1. Observational parameters.

a. Data acquisition system.

Receiver	Cooled parametric amplifier combined with a Dicke-switch
Backend: until August 1983	1-channel digital detector
since September 1983.....	2-channel multiplex digital detector
T_{sys}	200 K
HPBW of the antenna	2.66
T_B/S	0.453 K in T_B/Jy (for 2.66 beam)
Bandwidth	500 MHz

b. Center frequencies.

Observing period	Center frequency
March 1983–June 1983	10.05 GHz
September 1983–September 1984	10.55 GHz
September 1984–June 1986	10.05 GHz, 10.55 GHz

c. Flux Density Calibrators.

Observing period	Calibrator	Flux density
1984–1986	NGC 7027	6.61 Jy at 10.55 GHz
		6.65 Jy at 10.05 GHz
March–June 1983	3C 348	4.10 Jy at 10.05 GHz*
June 1983	3C 48	2.82 Jy at 10.05 GHz
April 1983	3C 123	7.94 Jy at 10.55 GHz

* Peak flux density with 2.66 beam.

$l \leq 358^\circ$ region, which was observed only at 10.05 GHz. About 40% of the whole area was observed at both frequencies. We combined all the data to make a final survey map.

The half-power beamwidth of the 45-m telescope was 2.66 at 10 GHz. The antenna beam pattern was well fitted by a Gaussian pattern and the side-lobe level was less than -16 dB of the peak intensity. The conversion factor from main beam flux density to main beam brightness temperature T_B is 0.453 K=1 Jy. Figure 1 shows the antenna response pattern to a point source, which was obtained from a map of NGC 7027.

The final map was made by joining many maps each of which was obtained at one observational sequence of scans. (Hereafter we refer to the small maps as element maps.) The typical size of an element map is $\Delta l \times \Delta b = 3^\circ \times 2^\circ$. Each element map was acquired by raster scans of 60° inclination from the north (in the equatorial coordinates) toward the west (position angle = -60°), in order to scan almost perpendicularly to the galactic plane. The length of each scan was $3^\circ 0$ or $3^\circ 2$. Only for $-2^\circ 0 \leq l \leq +2^\circ 0$ and some areas where strong sources exist near $b = +1^\circ 5$ or $-1^\circ 5$, the scan length was $4^\circ 0$. Several element maps were obtained by taking $2^\circ 0$ or $2^\circ 14$ scans. Each scan took 50 s and the scan separation was $0^\circ 02$. About a half of the survey area was observed more than twice. The rms noise in the resultant map was 30–140 mJy/beam or 14–63 mK in T_B depending mainly on weather conditions. Table 1 lists observational parameters of the survey.

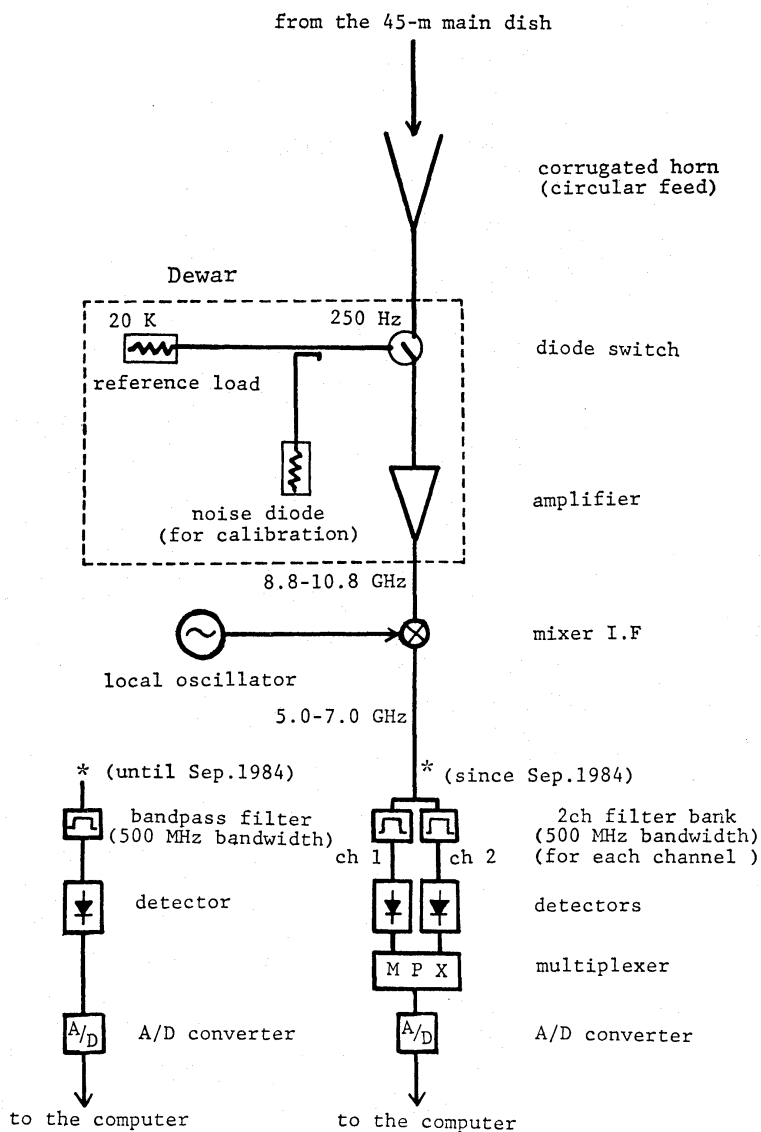


Fig. 2. The 10-GHz receiving system used at the NRO 45-m telescope.

The total intensity was obtained by using a circularly polarized feed and assuming that the circular polarization of the radiation is negligibly small.

The source NGC 7027 was used as the primary calibrator for flux density, and was assumed to be 6.65 and 6.61 Jy at 10.05 and 10.55 GHz, respectively, based on the spectrum of Andrew et al. (1981). The sources 3C 348, 3C 48, and 3C 123 were used as the flux calibrators until June 1983. The flux density of 3C 48 was assumed to be 2.82 Jy at 10.05 GHz based on the spectrum of Andrew et al. (1981). The peak flux density of 3C 348 was assumed to be 4.10 Jy/beam at 10.05 GHz using the NRO 45-m telescope (H. Tabara and T. Kato, private communication). The flux density of 3C 123 was assumed to be 7.94 Jy at 10.55 GHz based on the spectrum of Andrew et al. (1981).

The receiver gain fluctuation in a time scale of 10–20 min was calibrated by measuring the intensity of a standard noise diode.

Figure 2 shows a block diagram of the receiver system of the 45-m telescope. The

receiver consists of cooled parametric amplifiers followed by FET amplifiers.

3. Data Reduction

The first stage reduction was performed by using the CONDUCT system. This is a standard data reduction system for continuum observations at NRO on a FACOM M380S computer. A part of the CONDUCT system uses the NOD2 subroutine package (Haslam 1974). The CONDUCT system will be described in a separate paper.

For maps with a scan length $3^{\circ}0\text{--}4^{\circ}0$, both ends of each scan were assumed to be zero level. Then the element maps were checked by inspection to see whether or not emission at either end of the scans is really negligible. If any source exists, then the new base level was set by linear interpolation between the two lowest intensity points along the scan. Finally the PRESS method (Sofue and Reich 1979) was applied to suppress the scanning effects.

For maps with a scan length $2^{\circ}0\text{--}2^{\circ}14$, base levels were set using the maps made by combining the maps with a scan length $3^{\circ}0\text{--}4^{\circ}0$. The survey map was combined with all these element maps weighted by the inverses of the squares of the noise levels, and was constructed to have a $0^{\circ}02$ square grid referred to galactic coordinates. The final map was convolved by a Gaussian beam as if observed with $3^{\circ}0$ beam to improve the signal to noise ratio. After the convolution the rms noise level of the map is 10–40 mK in T_B (typically 15 mK). The conversion factor from flux density to brightness temperature T_B is $0.356 \text{ K} = 1 \text{ Jy}/3^{\circ}0 \text{ beam}$.

4. Results

a. Contour Maps of the Survey

In figures 3 to 33 the 10-GHz survey maps are shown in the form of contour maps of $2^{\circ}2 \times 3^{\circ}$ with 1° grids of galactic and equatorial coordinates (epoch 1950.0). The contour levels are as follows:

- 0.10 K to 1.00 K in 0.10 K step,
- 1.00 K to 3.00 K in 0.20 K step,
- 3.00 K to 5.00 K in 0.50 K step,
- 5.00 K to 10.00 K in 1.00 K step,
- 10.00 K to 20.00 K in 2.00 K step,
- 20.00 K to 50.00 K in 5.00 K step.

Some contours are labeled in relative brightness in kelvins or arrows which point towards local brightness minima. The contours without labels are not drawn where the contours are overcrowded. Notes to the individual maps are given in the captions of each figure.

b. A List of Small Diameter Sources

In table 2 we have listed 144 small-diameter radio sources detected in the survey area. The criteria for including the listed sources are as follows: (1) The apparent diameter at the full width of half maximum is smaller than $4^{\circ}5$ and larger than $2^{\circ}4$ (with $3^{\circ}0$ -beam). (2) The peak flux density is brighter than $0.3 \text{ Jy}/3^{\circ}0 \text{ beam}$. (3)

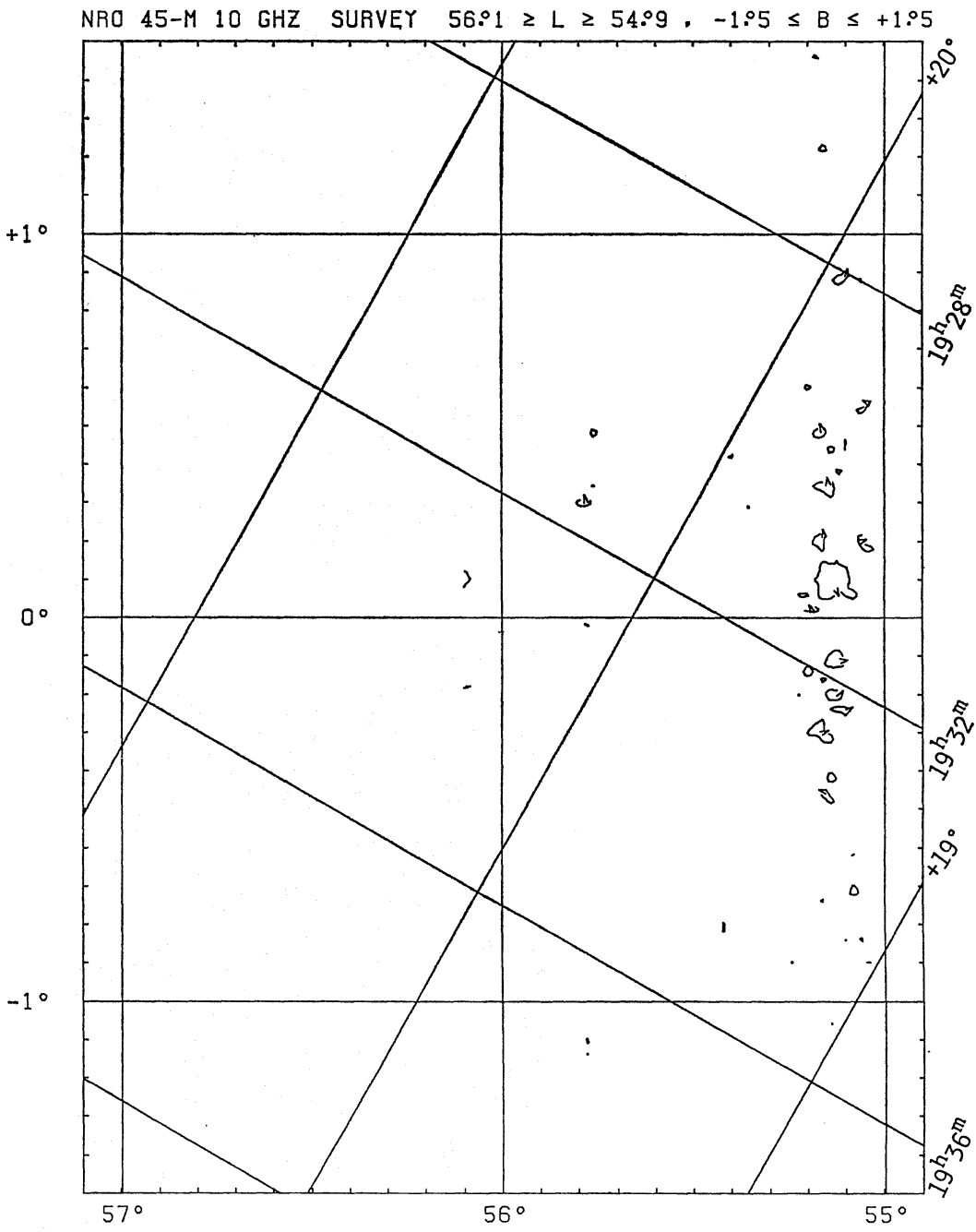


Fig. 3. The atlas of contour maps in galactic coordinates ordered by decreasing longitude. The labels on contours indicate brightness temperatures in kelvins. The region $L \geq 56^{\circ}1$ has not been observed. The noise level of this map is about 30 mK. Many weak features presented by the lowest contour may not be real.

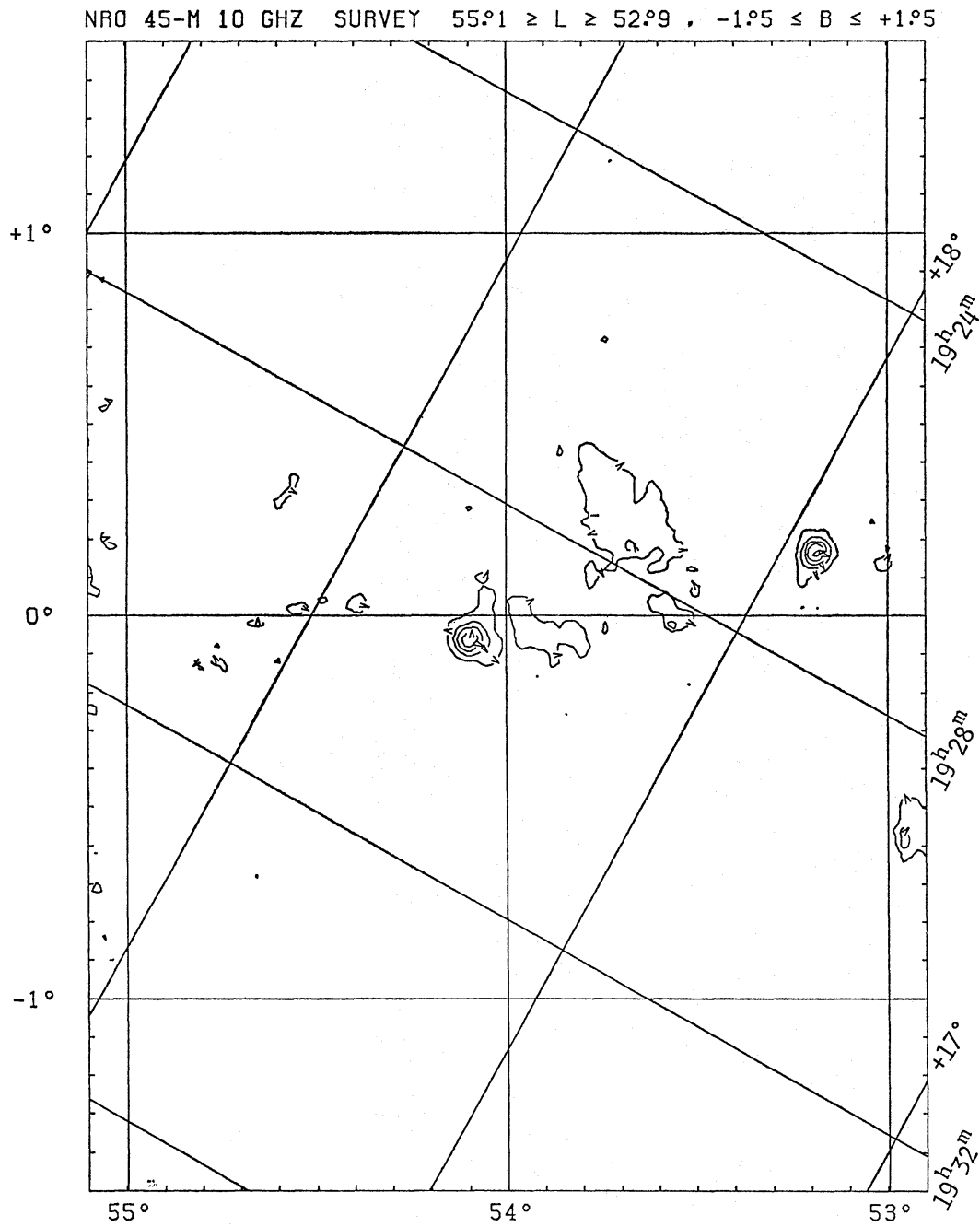


Fig. 4. See the caption of figure 3. The noise level of this map is about 20 mK. Many weak features presented by the lowest contour may not be real.

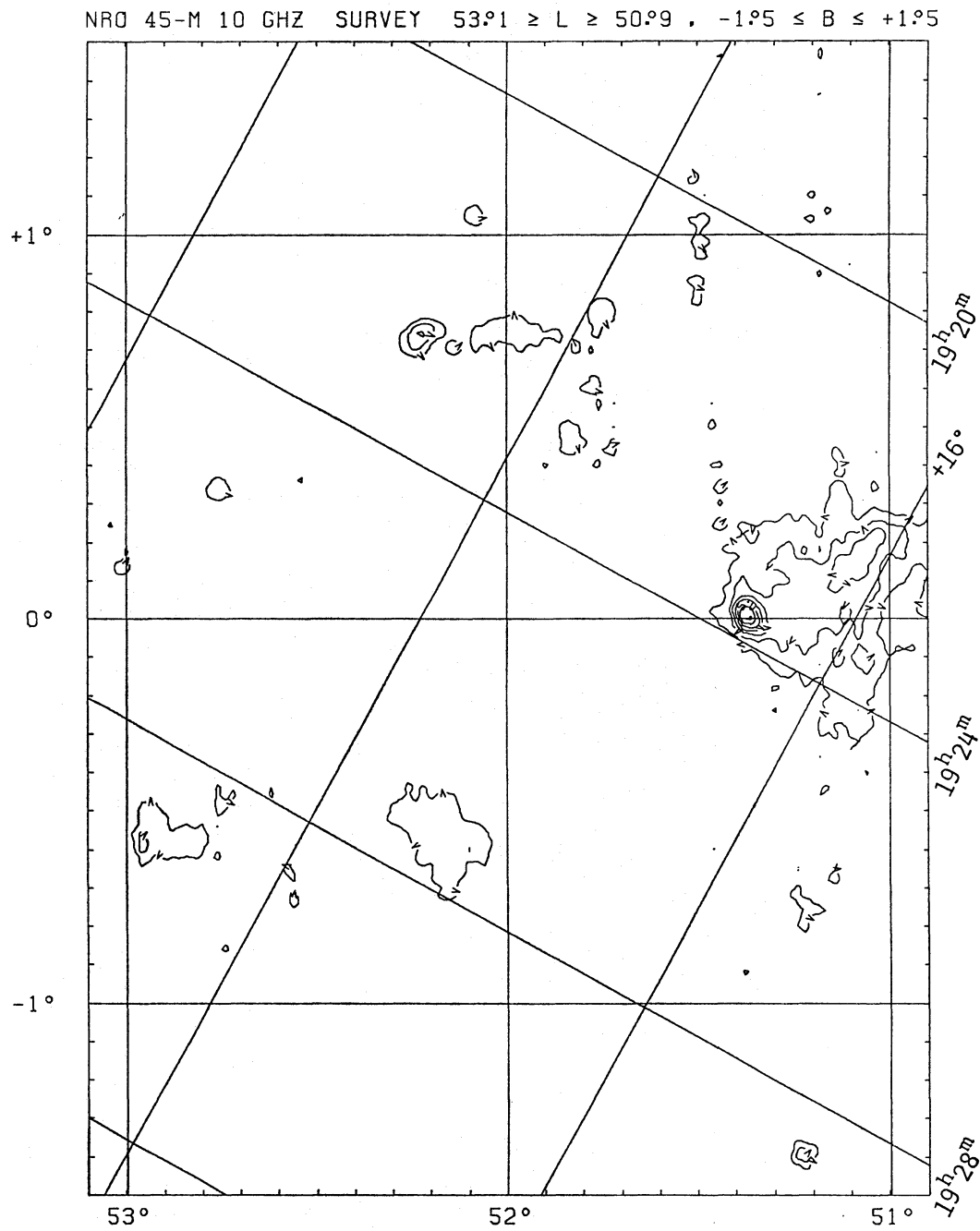


Fig. 5. See the caption of figure 3. The noise level of this map is about 25 mK. Many weak features presented by the lowest contour may not be real.

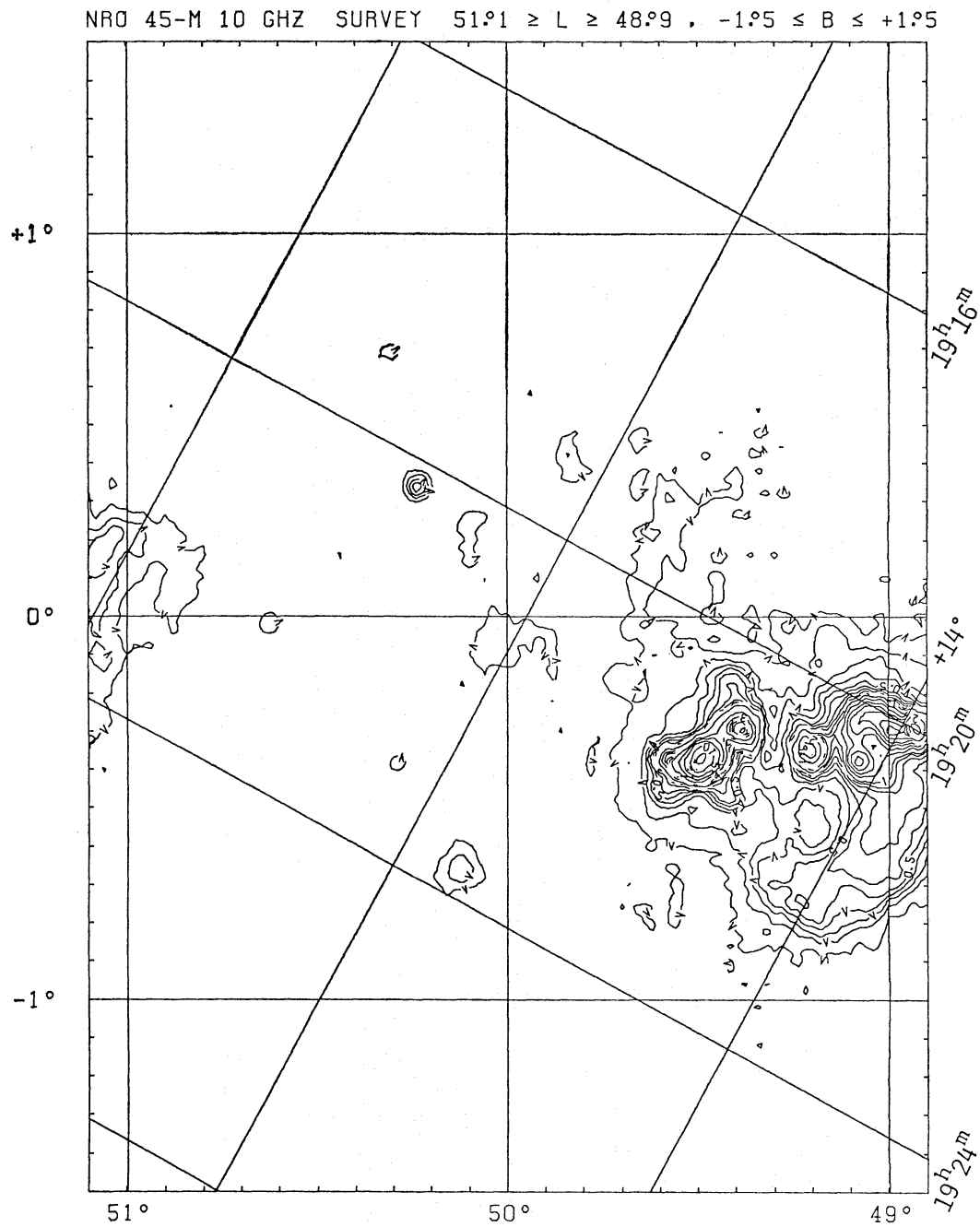


Fig. 6. See the caption of figure. 3 The noise level of this map is about 20 mK. Many weak features presented by the lowest contour in the region near $l \approx 49.4^{\circ}$ may not be real.

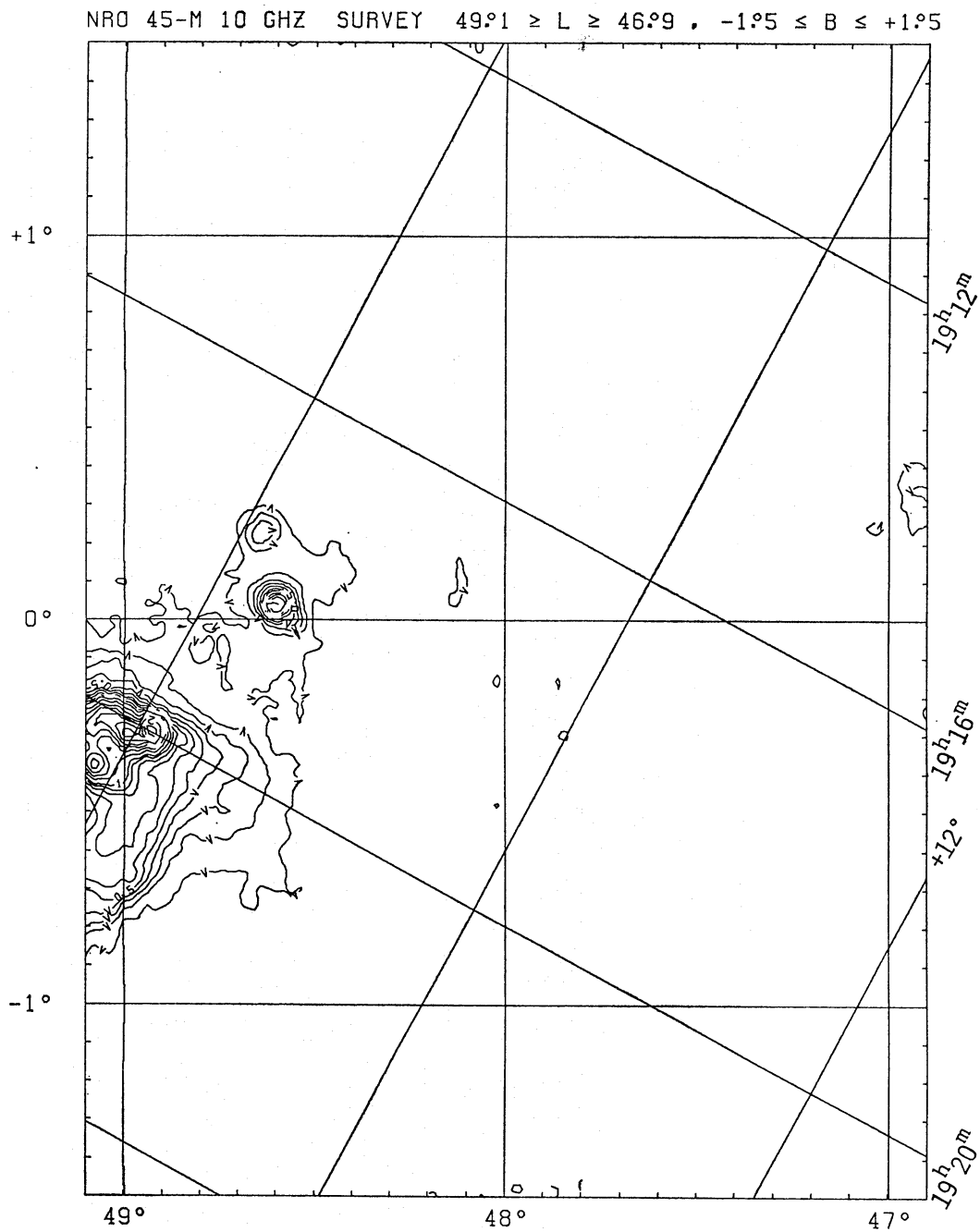


Fig. 7. See the caption of figure 3.

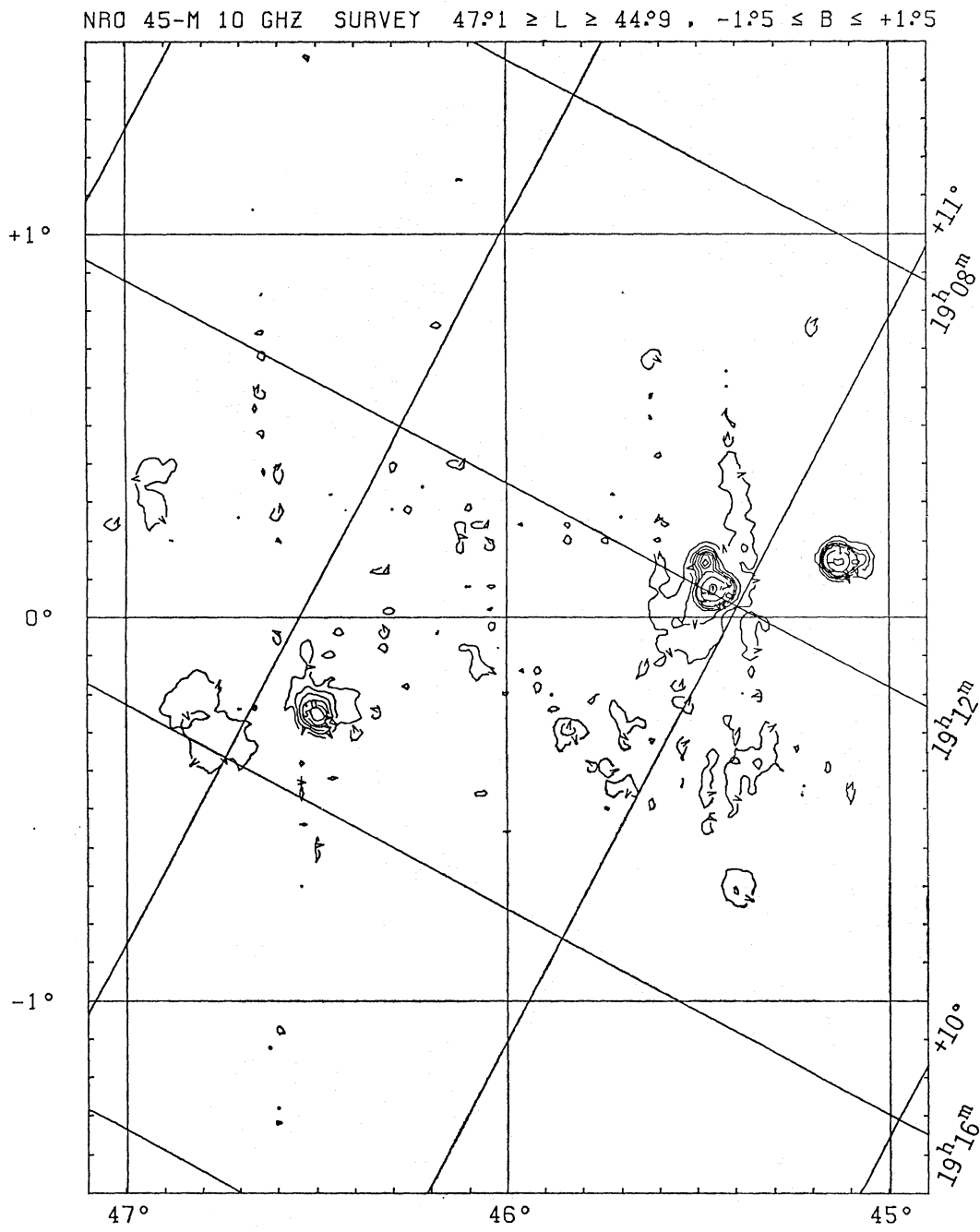


Fig. 8. See the caption of figure 3. The noise level of this map is about 20 mK. Many weak features presented by the lowest contour may not be real.

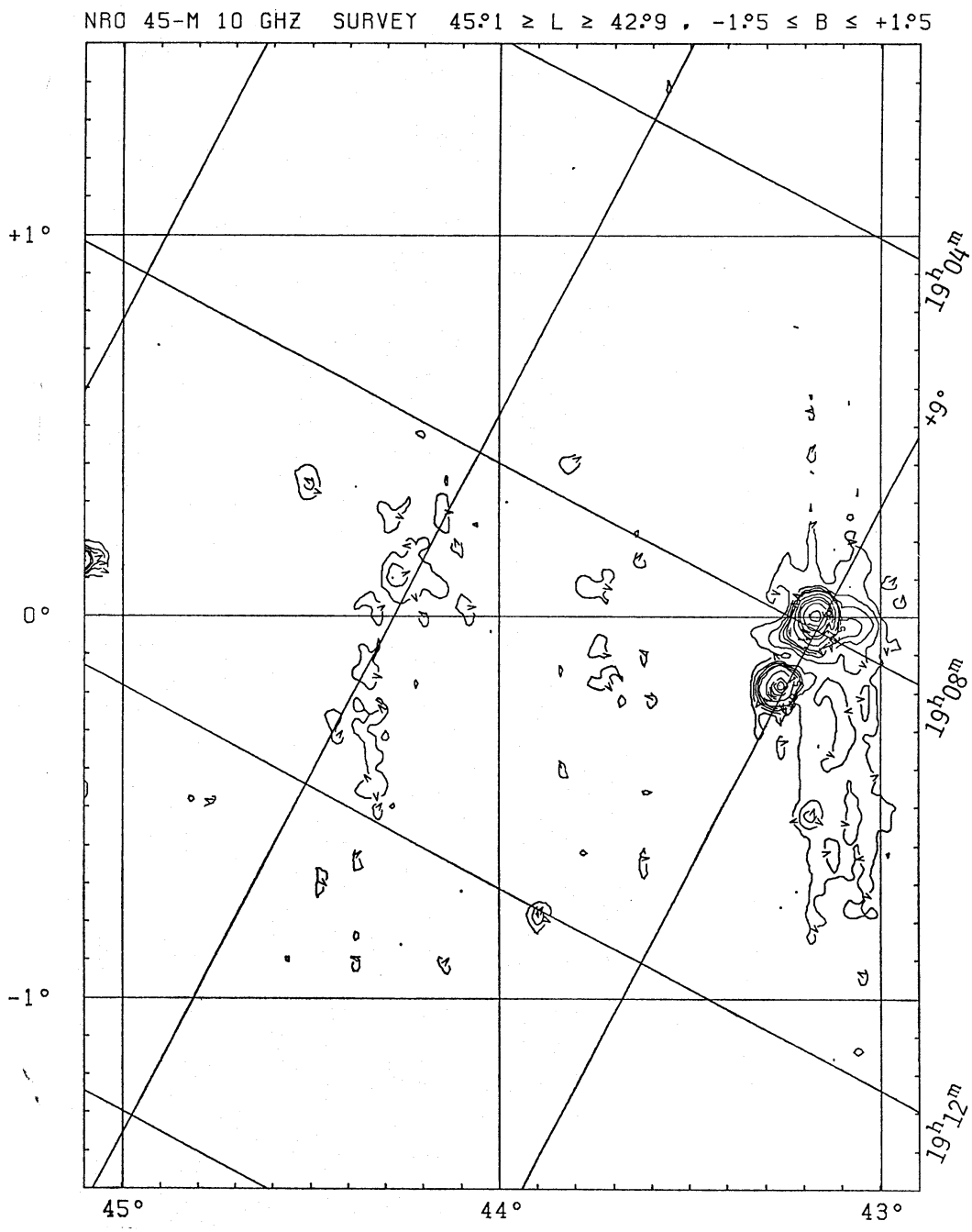


Fig. 9. See the caption of figure 3. The noise level of this map is about 25 mK. Many weak features presented by the lowest contour may not be real.

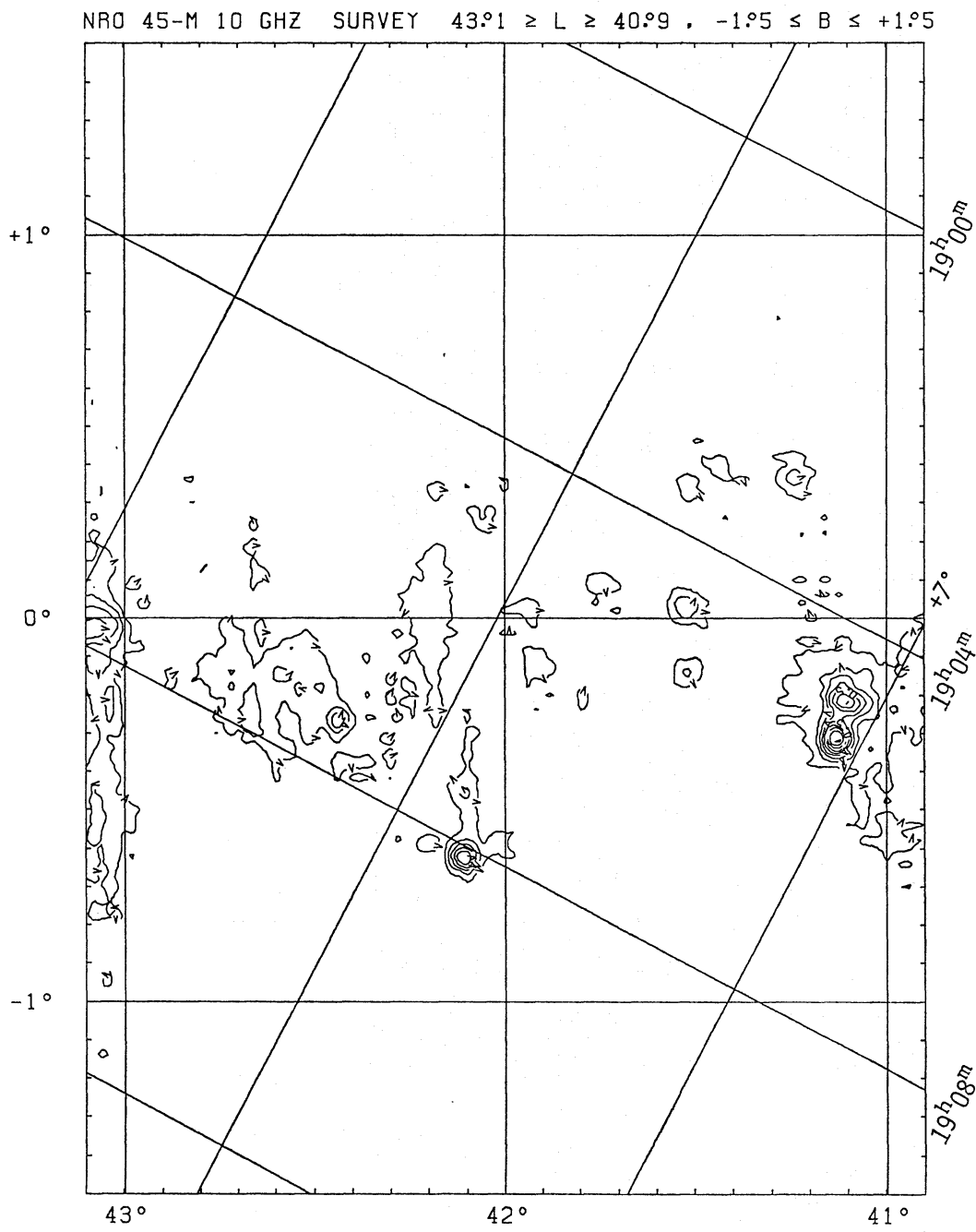


Fig. 10. See the caption of figure 3. The noise level of this map is about 25 mK. Many weak features presented by the lowest contour may not be real.

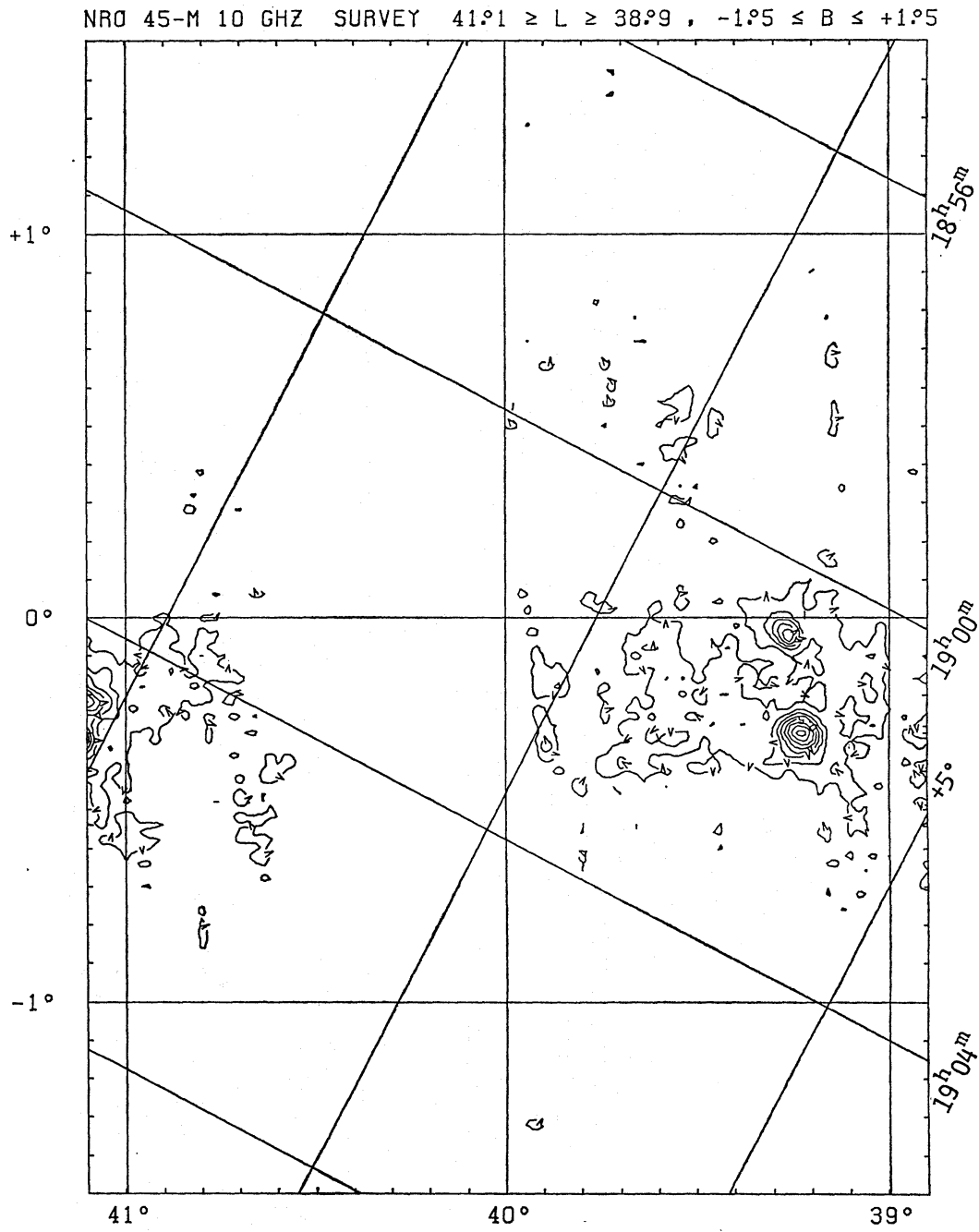


Fig. 11. See the caption of figure 3. The noise level of this map is about 20 mK. Many weak features presented by the lowest contour may not be real.

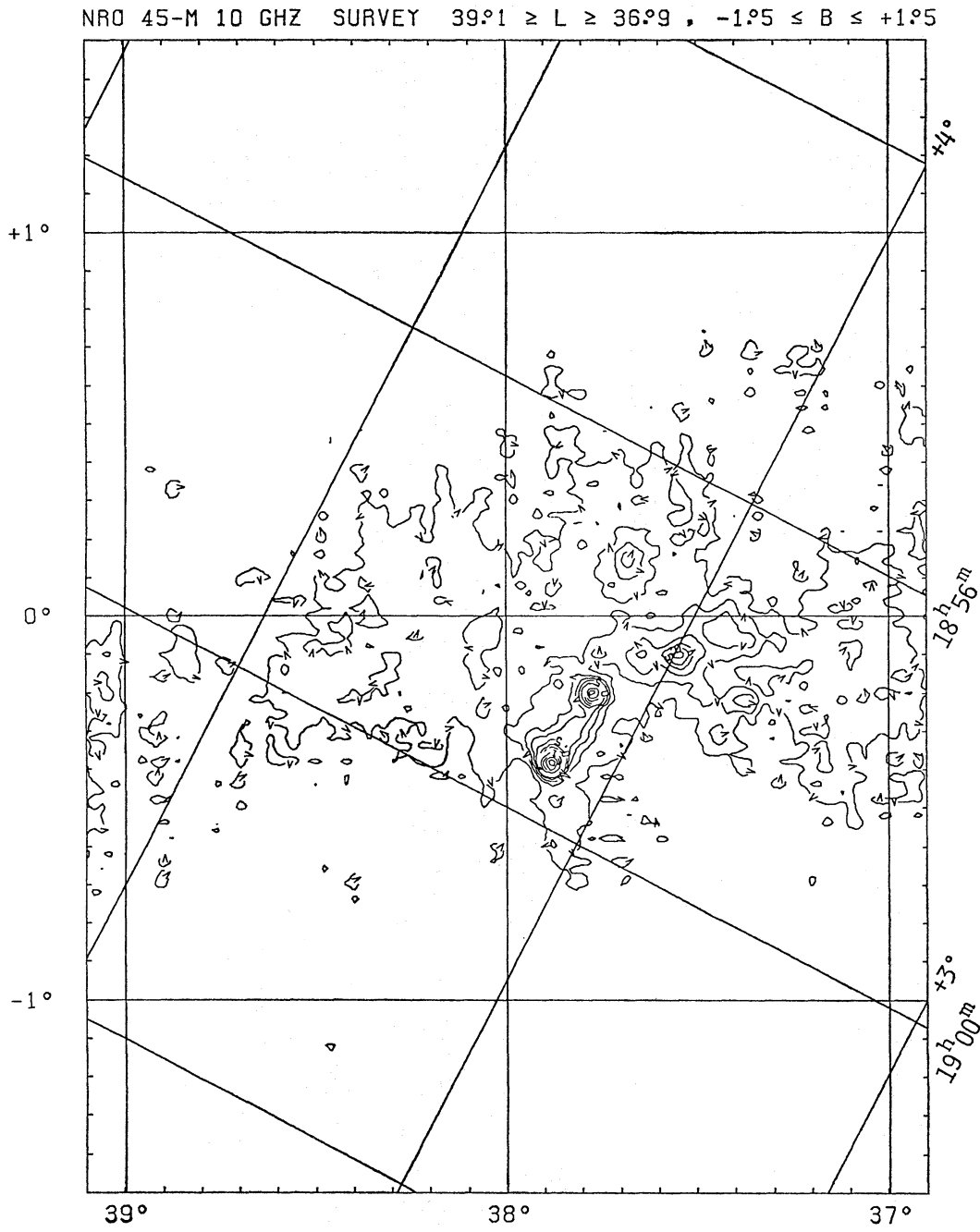


Fig. 12. See the caption of figure 3. The noise level of this map is about 25 mK. Many weak features presented by the lowest contour may not be real.

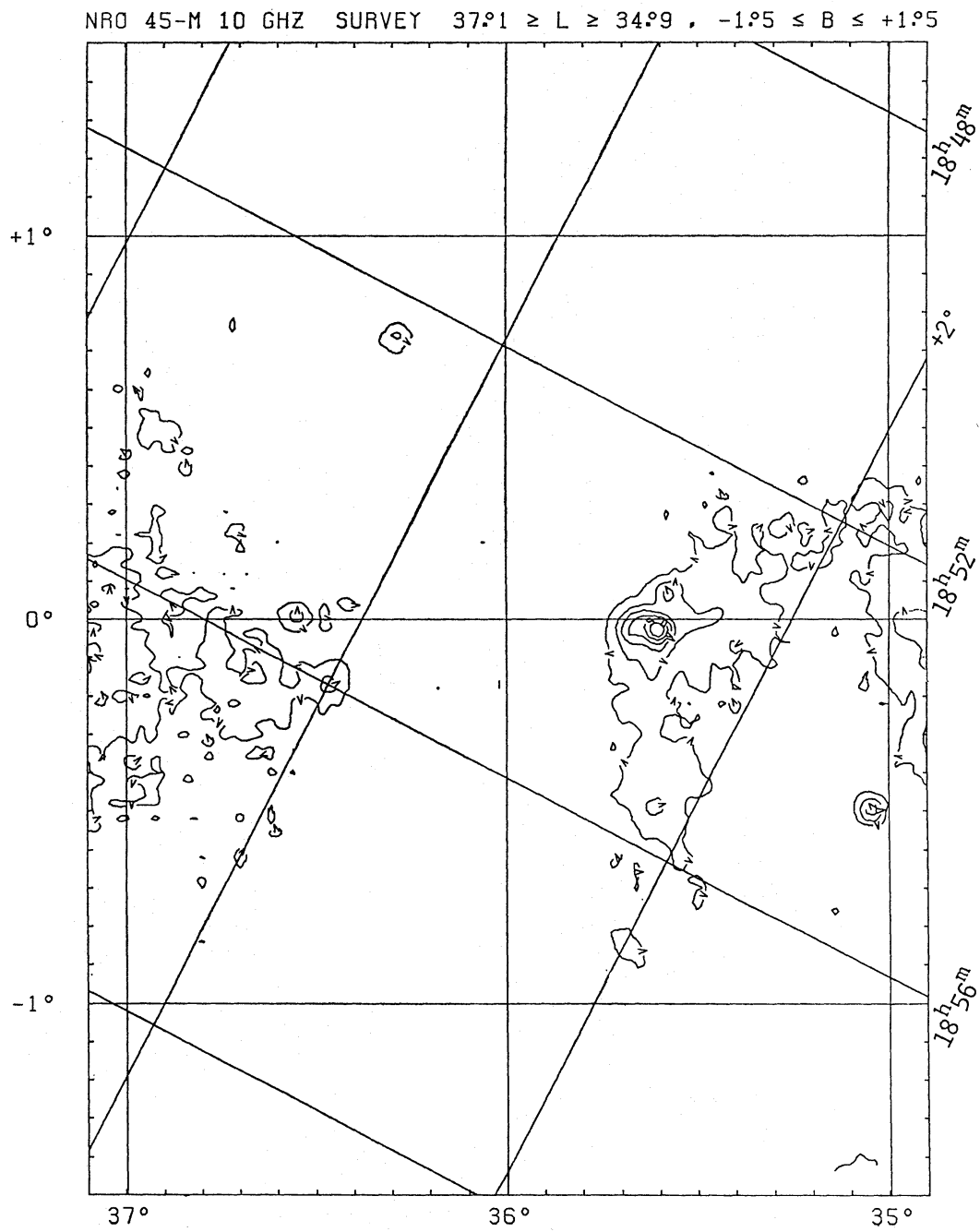


Fig. 13. See the caption of figure 3. The noise level of this map is about 20 mK. Many weak features presented by the lowest contour may not be real.

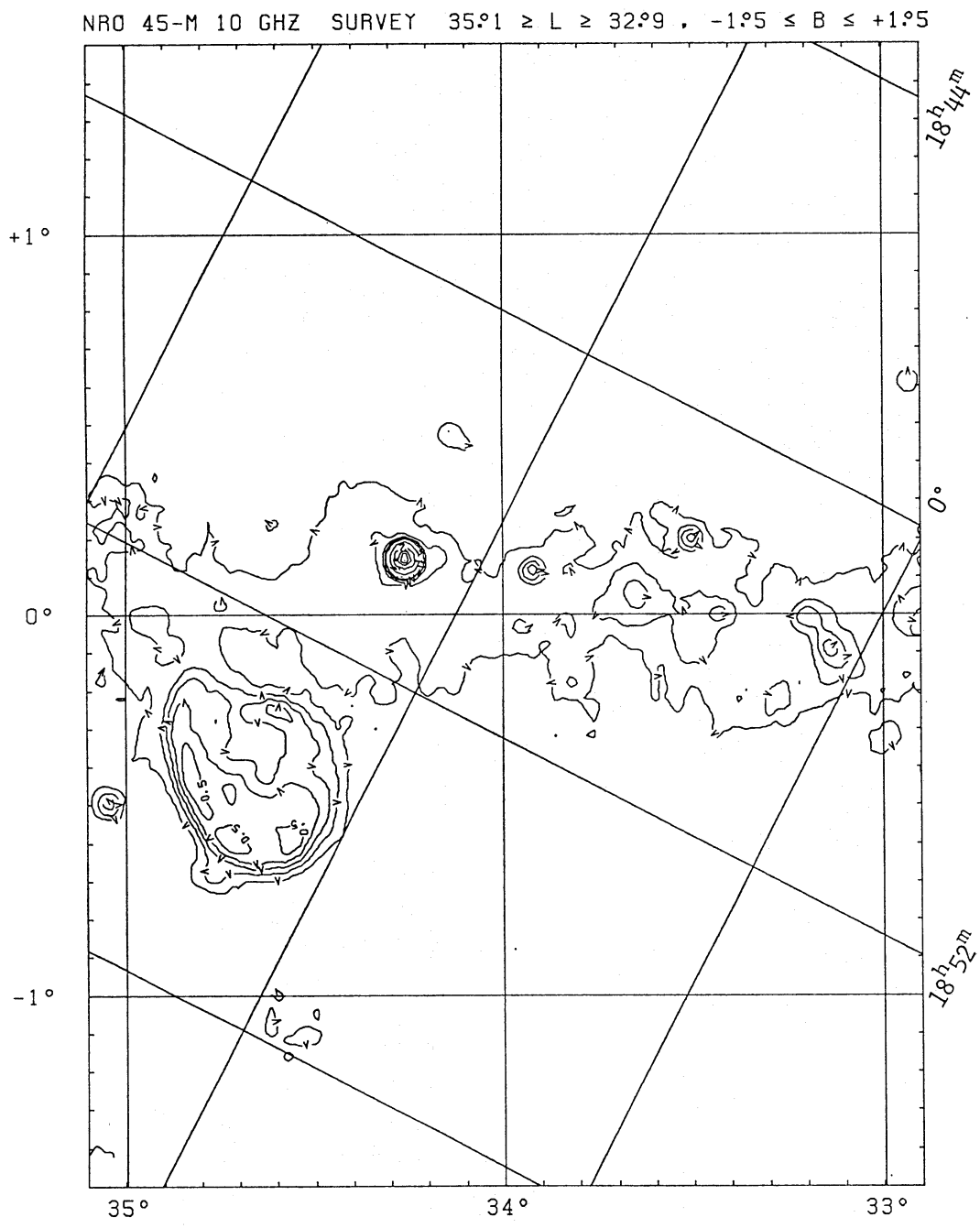


Fig. 14. See the caption of figure 3.

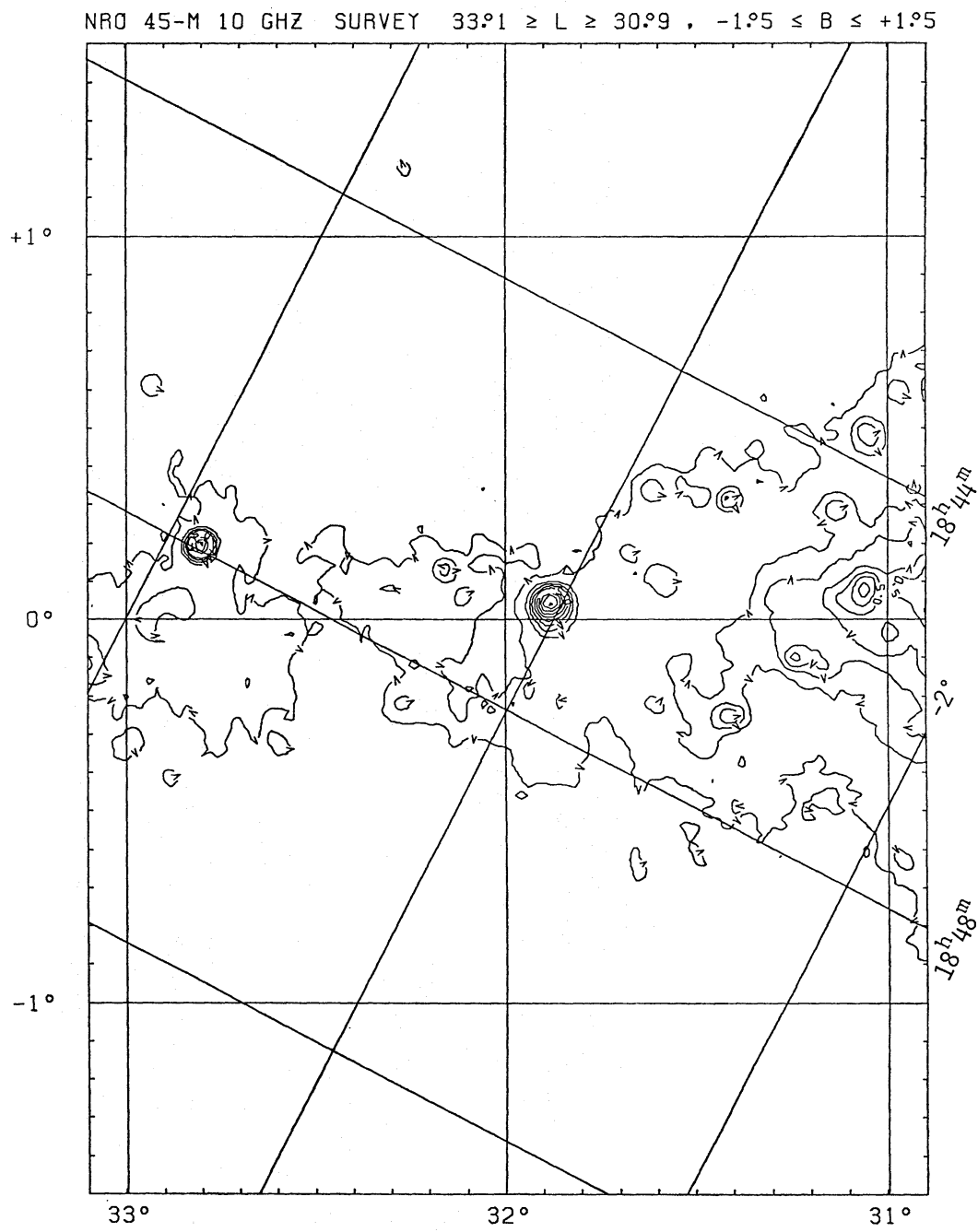


Fig. 15. See the caption of figure 3.

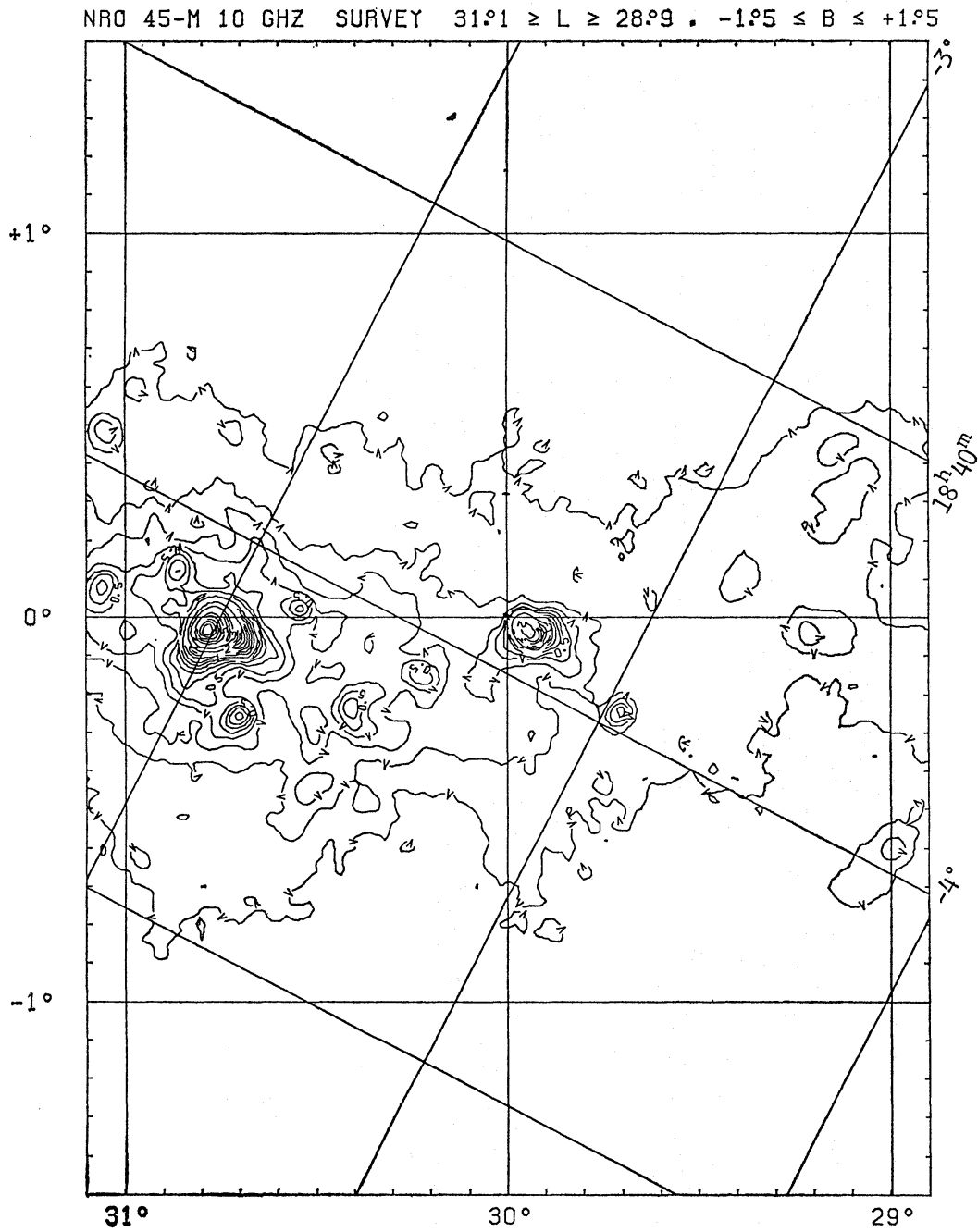


Fig. 16. See the caption of figure 3.

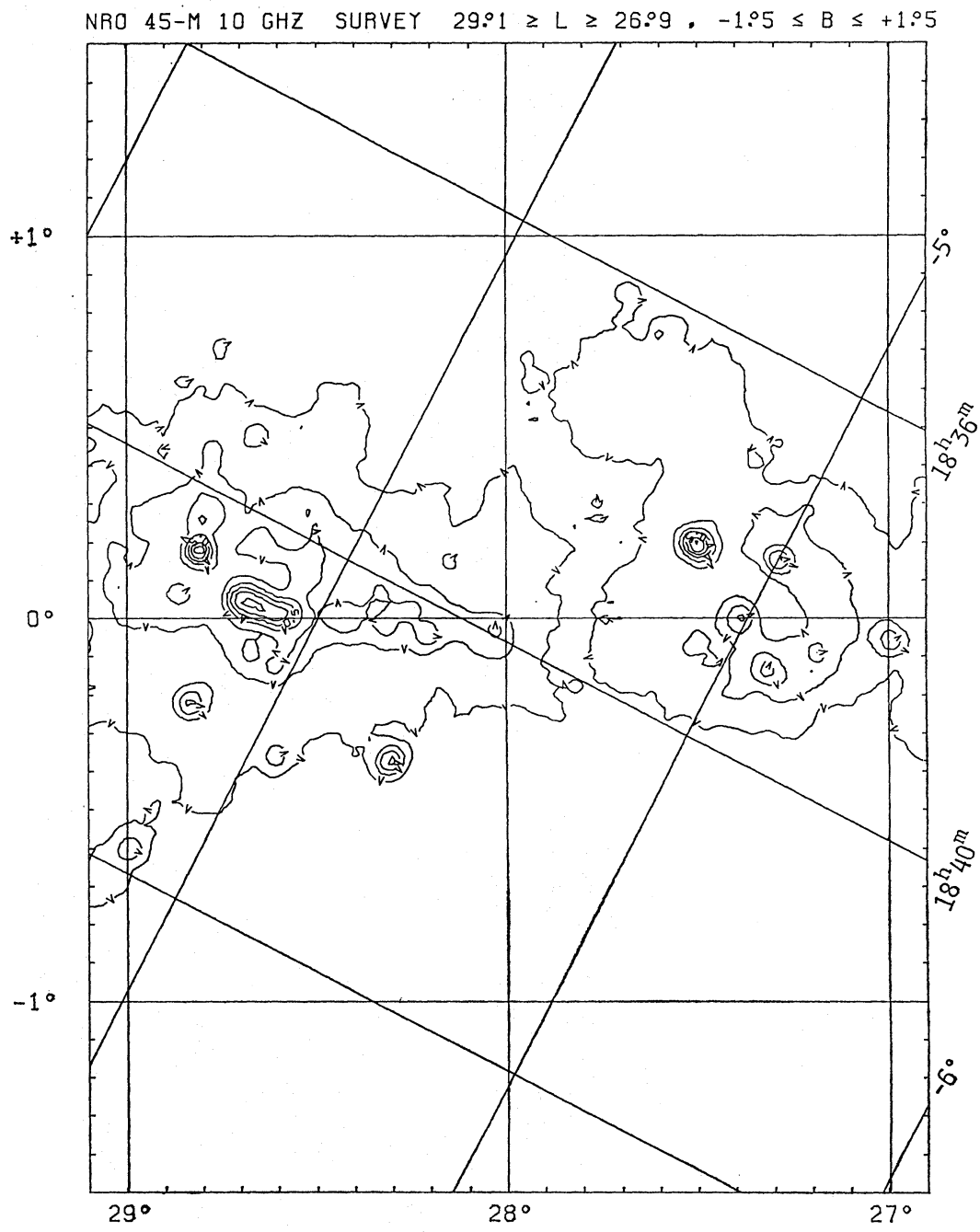


Fig. 17. See the caption of figure 3.

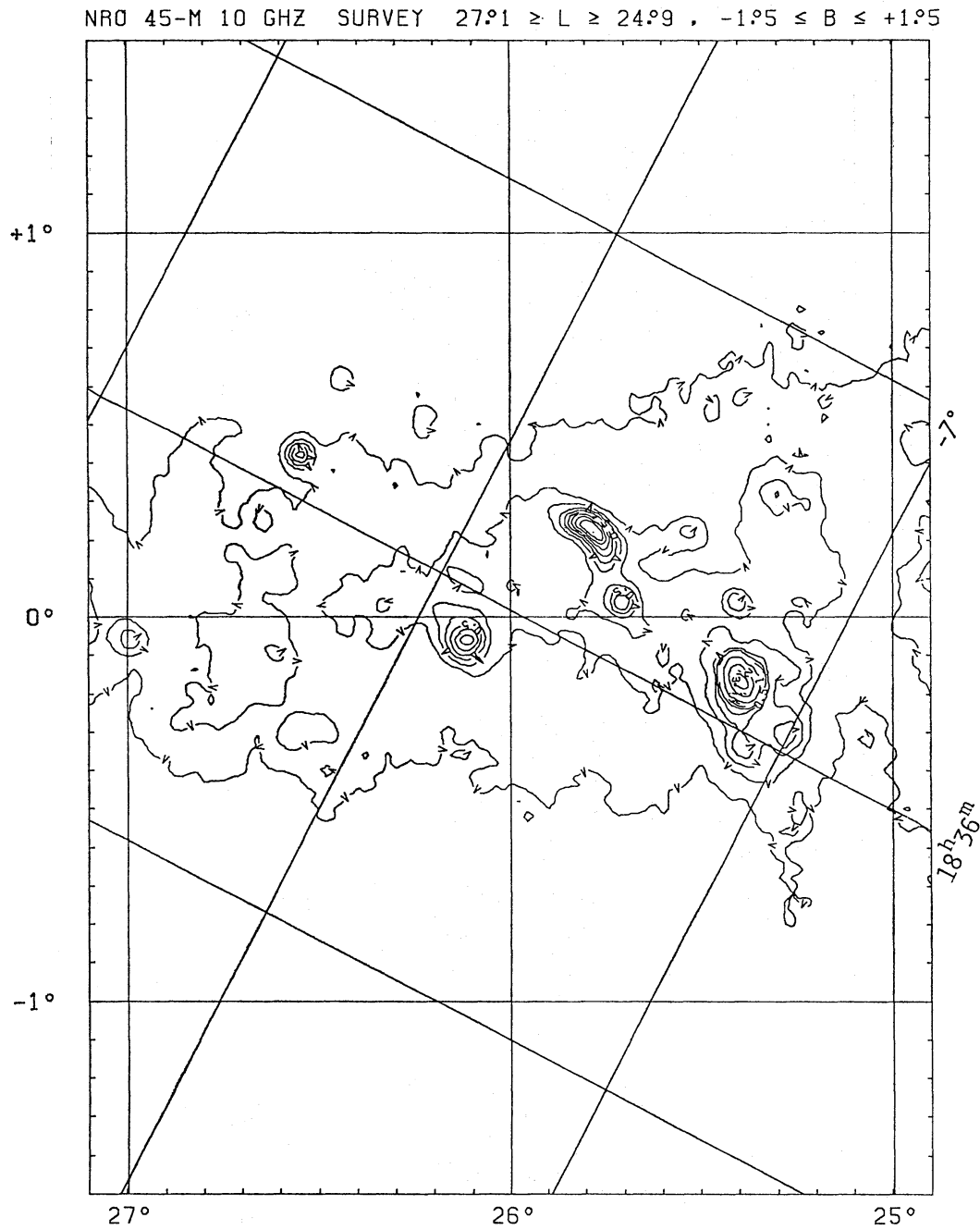


Fig. 18. See the caption of figure 3.

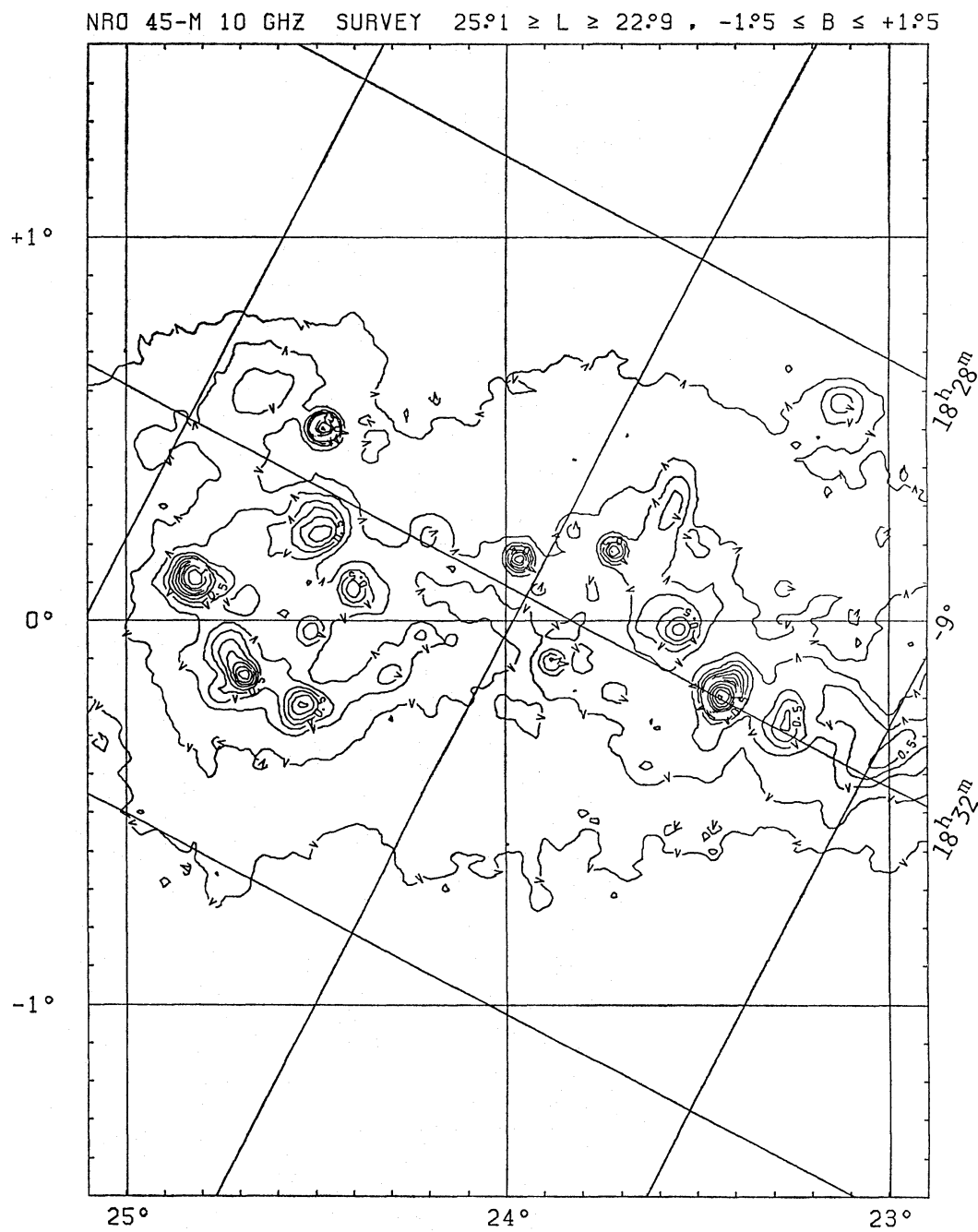


Fig. 19. See the caption of figure 3.

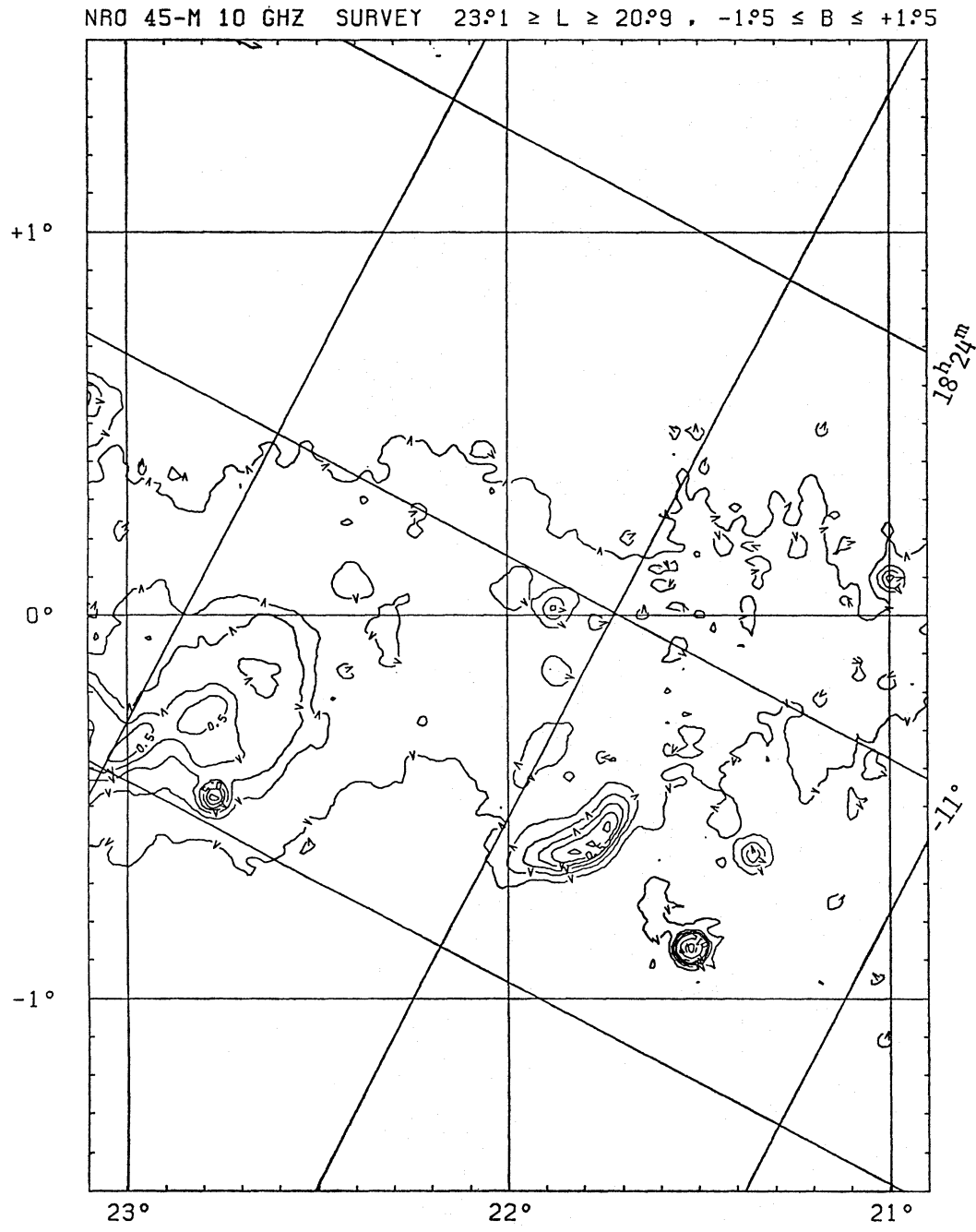


Fig. 20. See the caption of figure 3. The noise level of the region $21^{\circ}0 \leq l \leq 21^{\circ}6$ is about 25 mK. Many weak features presented by the lowest contour in this region may not be real.

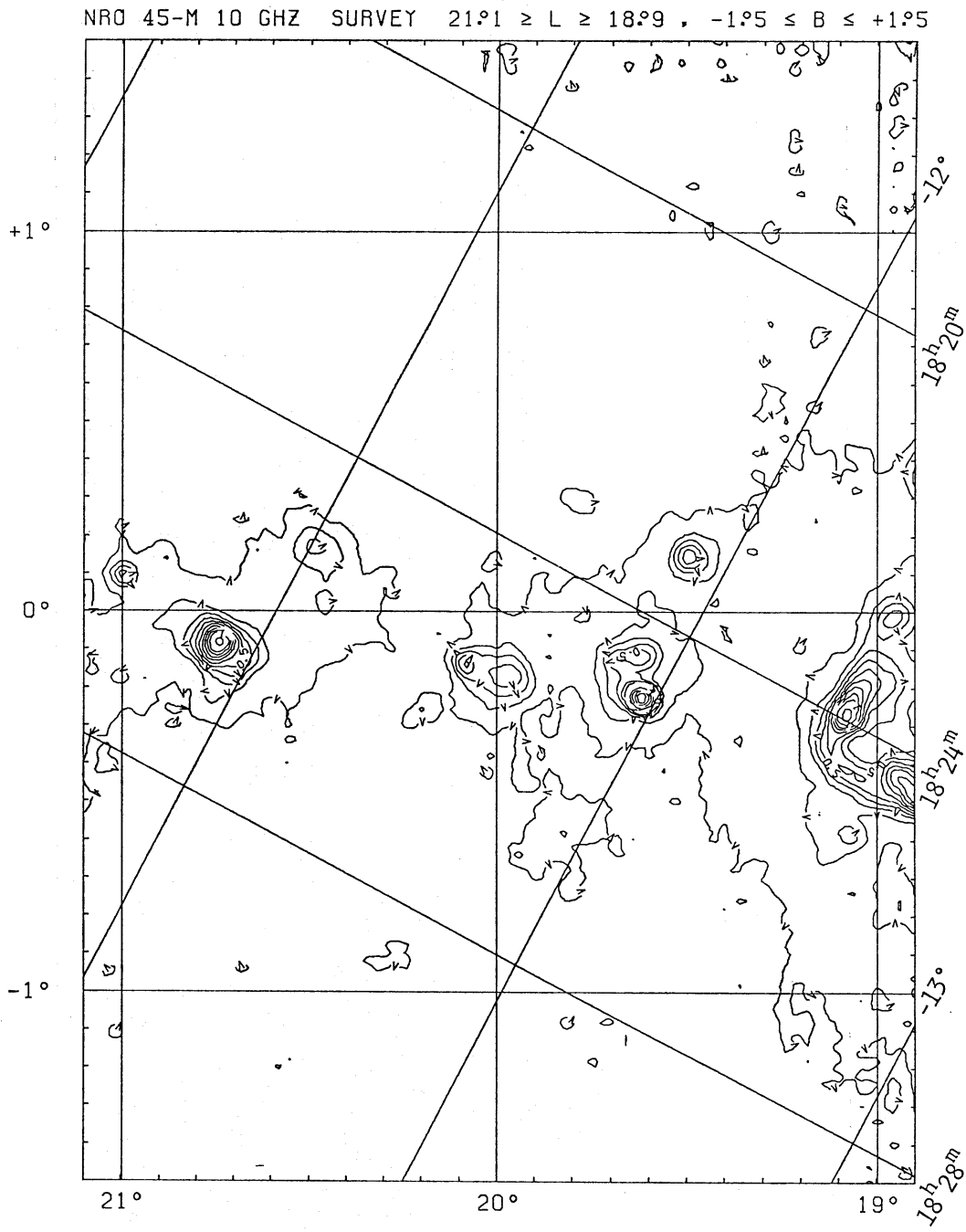


Fig. 21. See the caption of figure 3. The noise level of the region $l \leq 20^{\circ}0$, $|b| \geq 1^{\circ}0$ is about 30 mK. Many weak features presented by the lowest contour in this region may not be real.

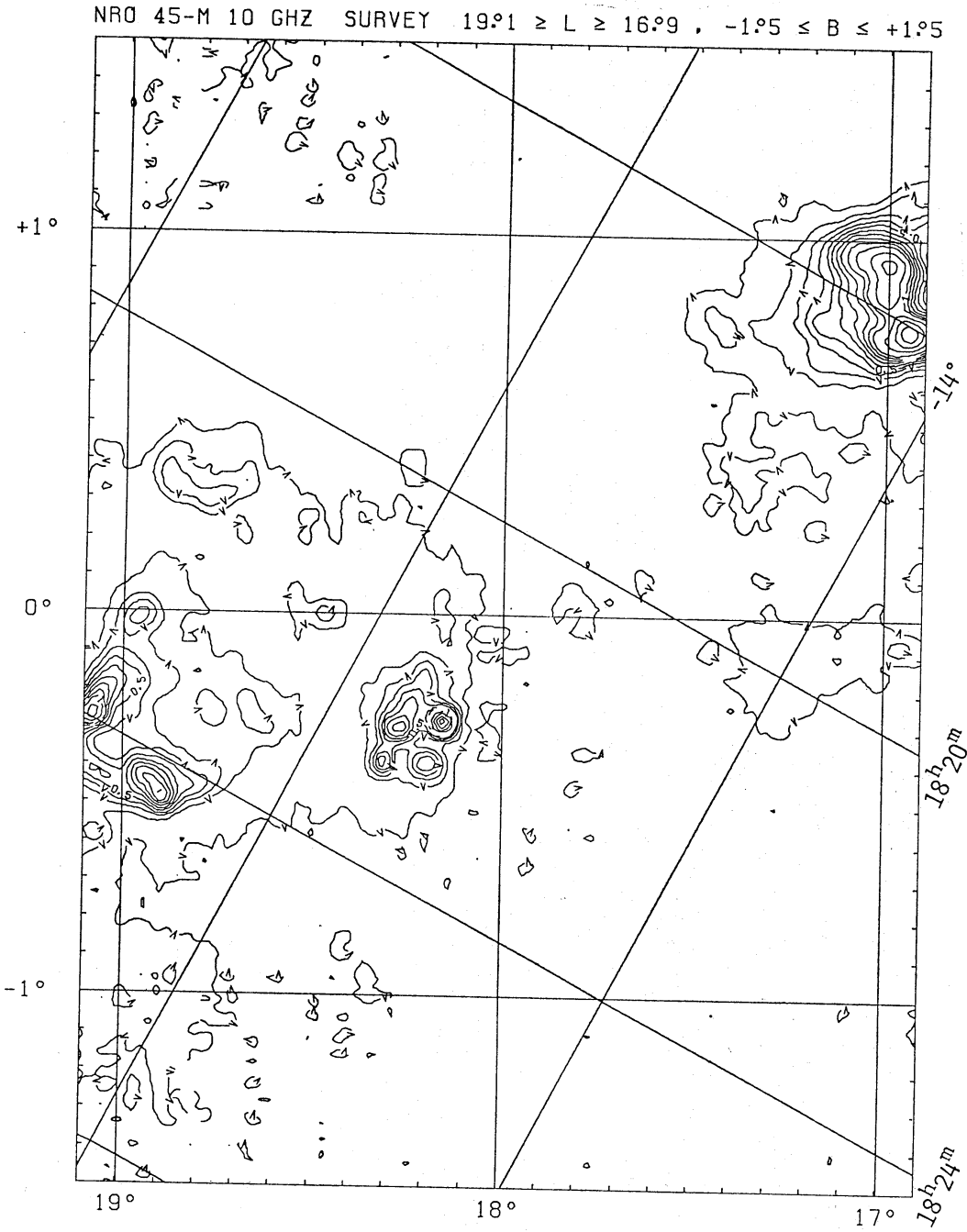


Fig. 22. See the caption of figure 3. The noise level of the region $l \geq 18.2^\circ$, $|b| \geq 1.0^\circ$ is about 45 mK. Many weak features presented by the lowest contour in this region may not be real.

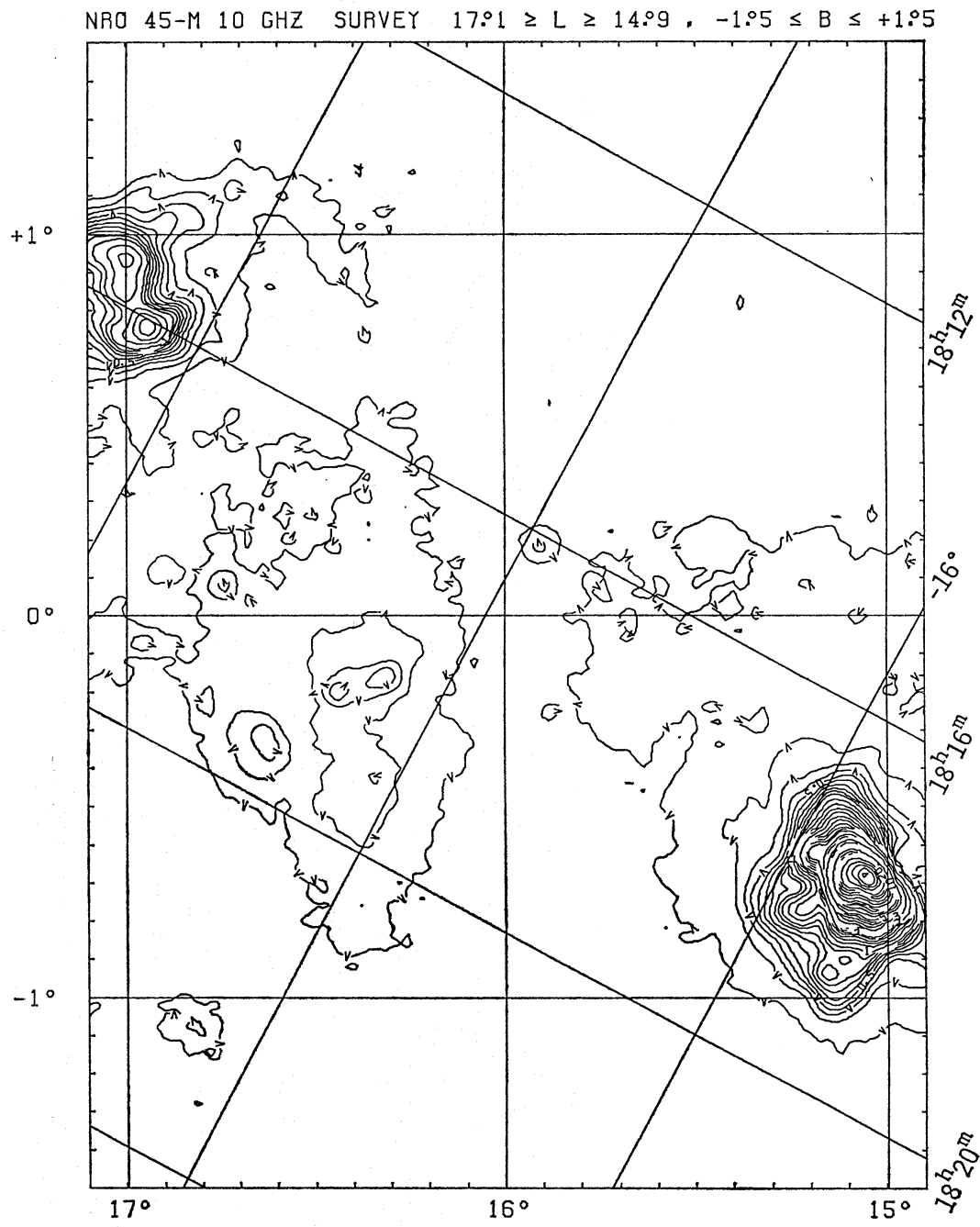


Fig. 23. See the caption of figure 3.

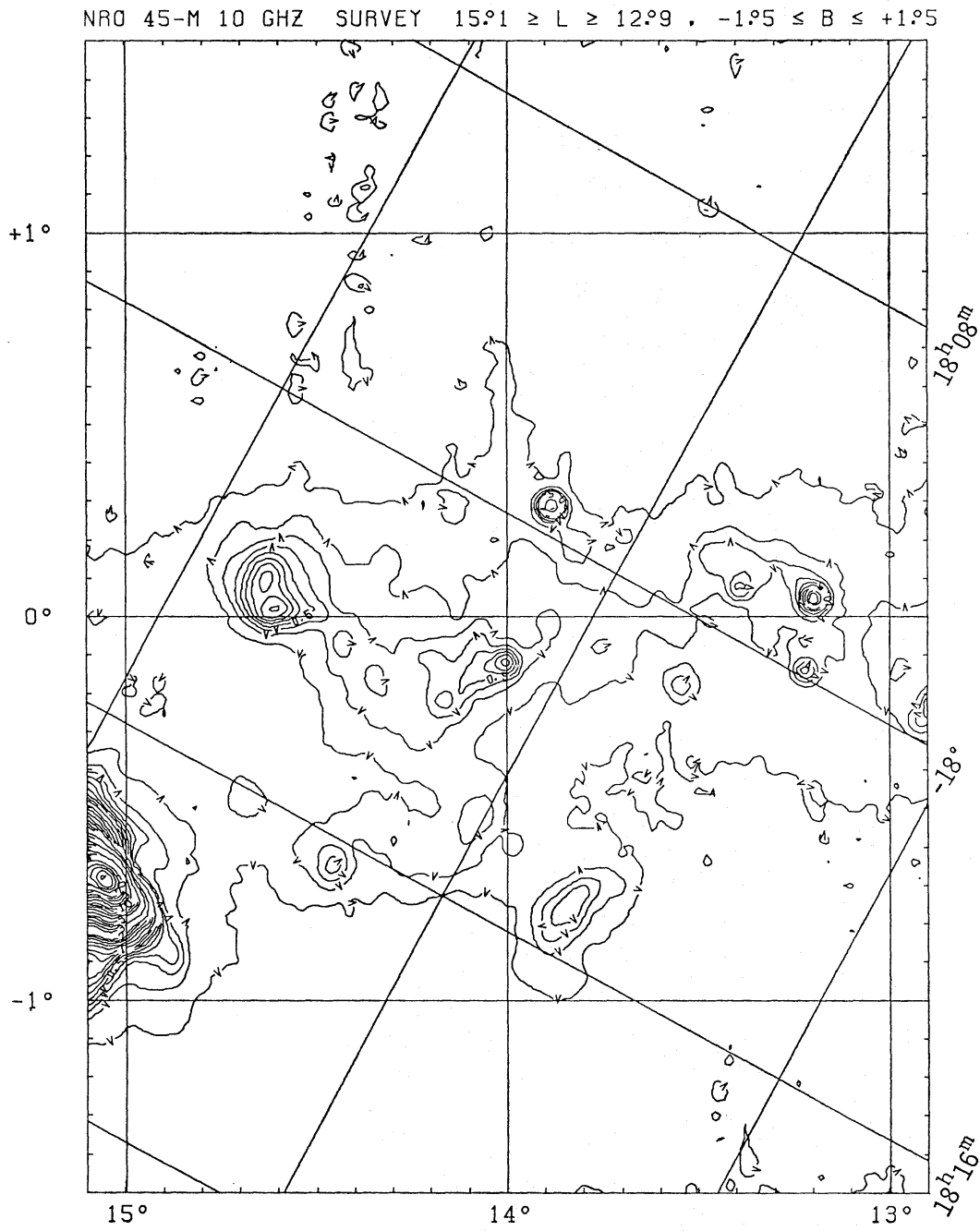


Fig. 24. See the caption of figure 3. The noise level of the region $L \leq 14^{\circ}0$, $b \geq +0^{\circ}5$ is about 30 mK. The noise level of the region $L \leq 14^{\circ}0$, $|b| \geq 1^{\circ}0$ is about 35 mK. Many weak features presented by the lowest contour in these regions may not be real.

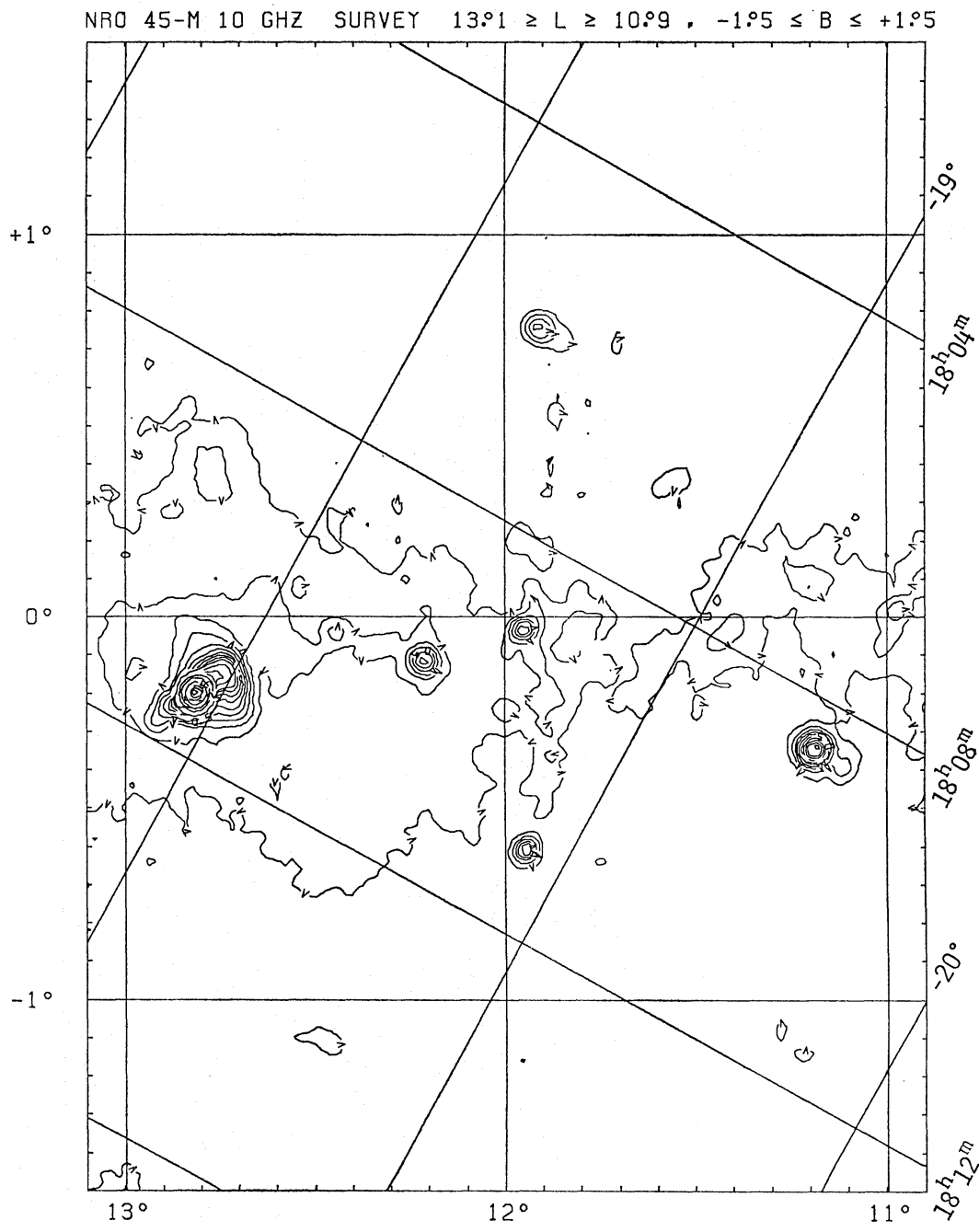


Fig. 25. See the caption of figure 3. Some weak features along galactic latitude near $l \approx 11.9^{\circ}$ presented by the lowest contour may not be real because of the unremovable scanning effect.

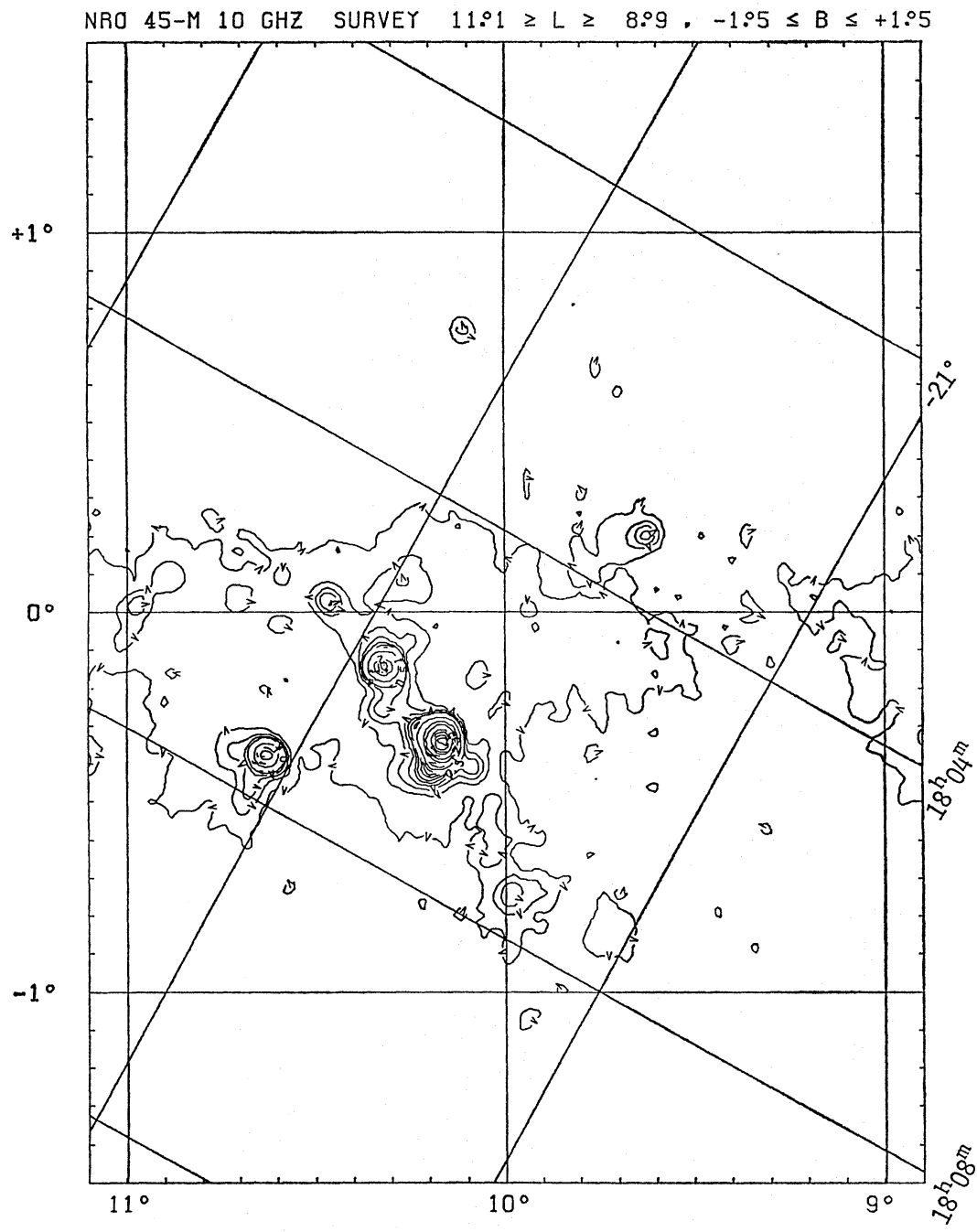


Fig. 26. See the caption of figure 3.

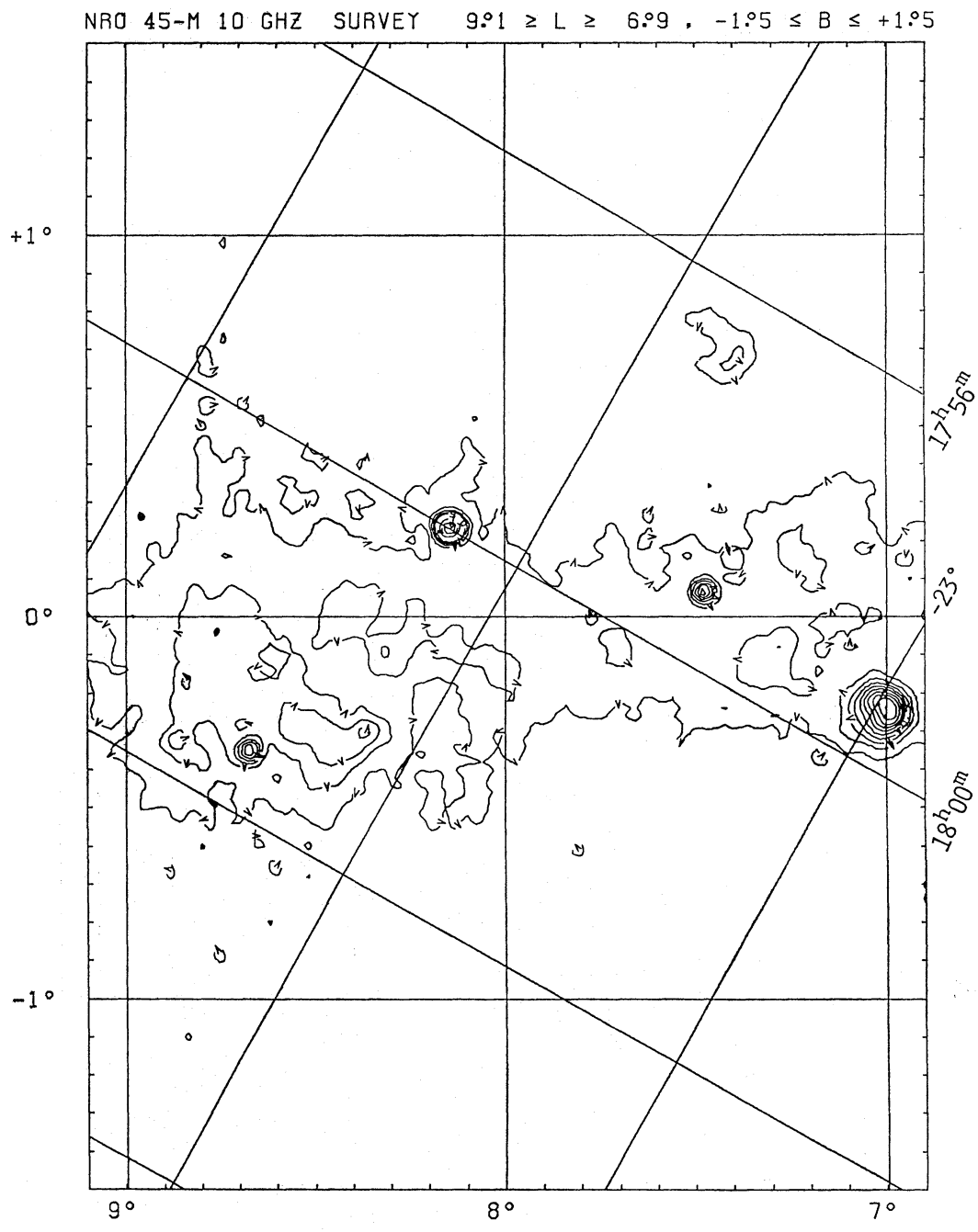


Fig. 27. See the caption of figure 3.

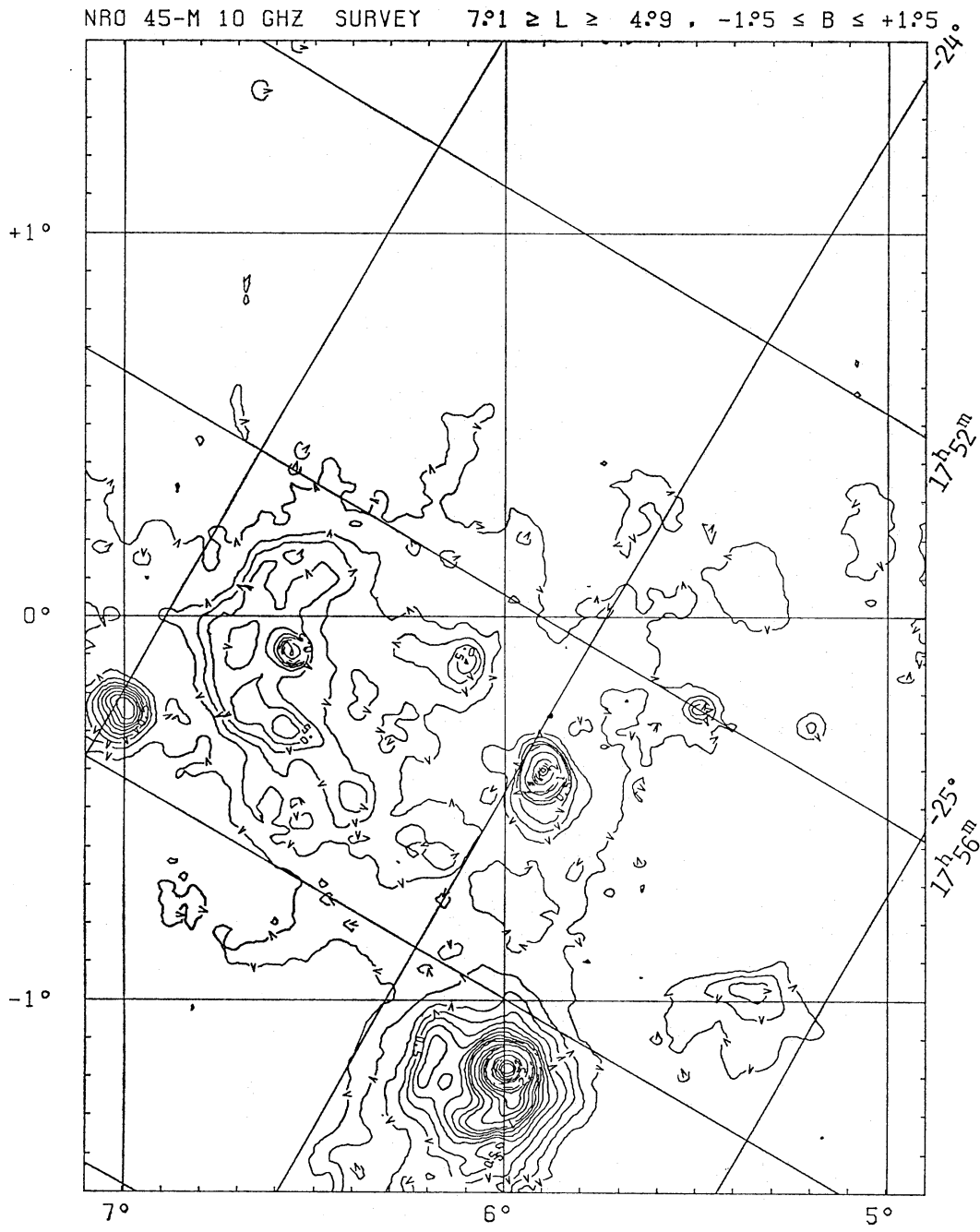


Fig. 28. See the caption of figure 3. The noise level of this map is about 25 mK. Many weak features presented by the lowest contour in this region may not be real.

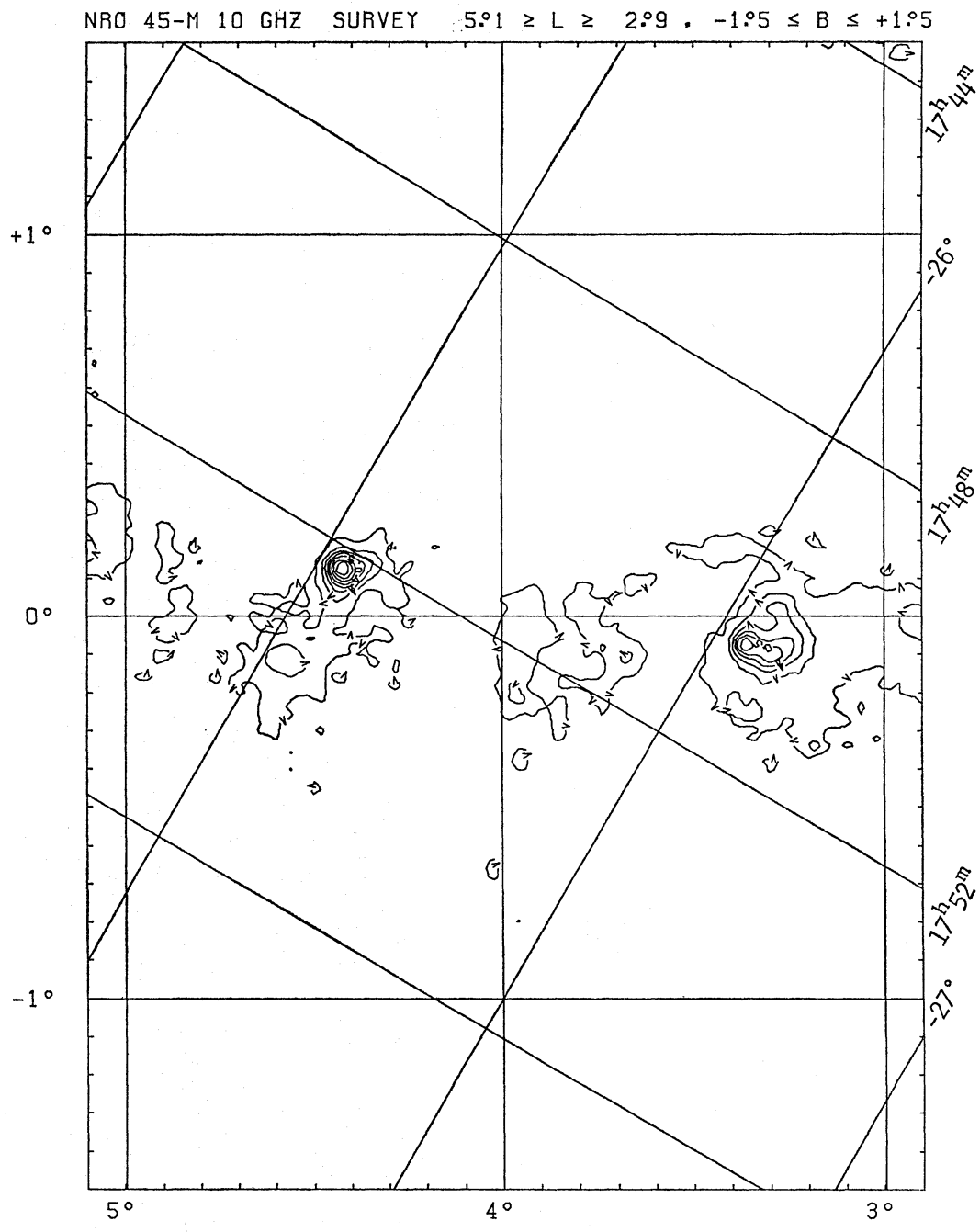


Fig. 29. See the caption of figure 3.

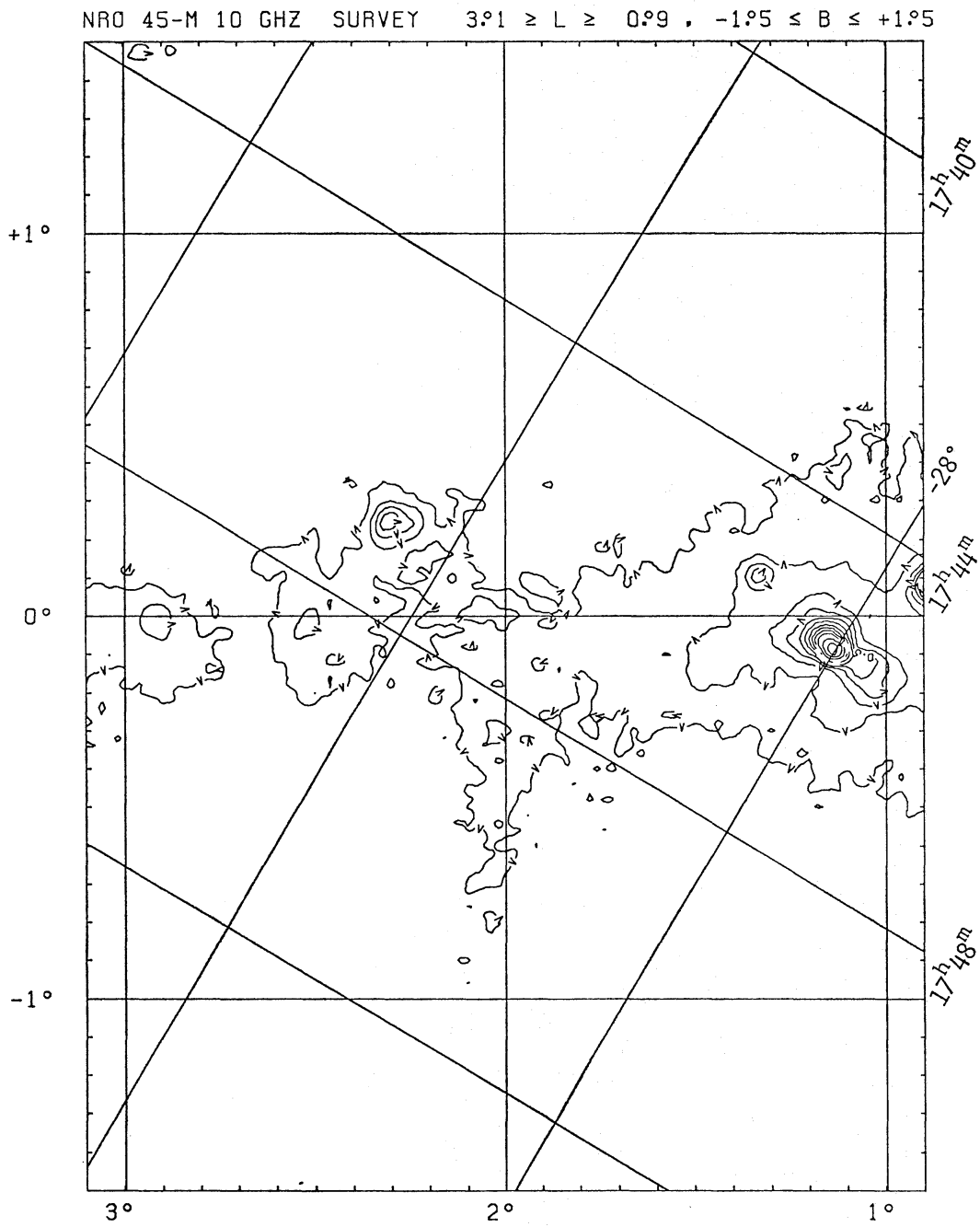


Fig. 30. See the caption of figure 3. Features along galactic latitude near $1^{\circ}9 \leq l \leq 2^{\circ}1$ may not be real because of the unremovable scanning effect.

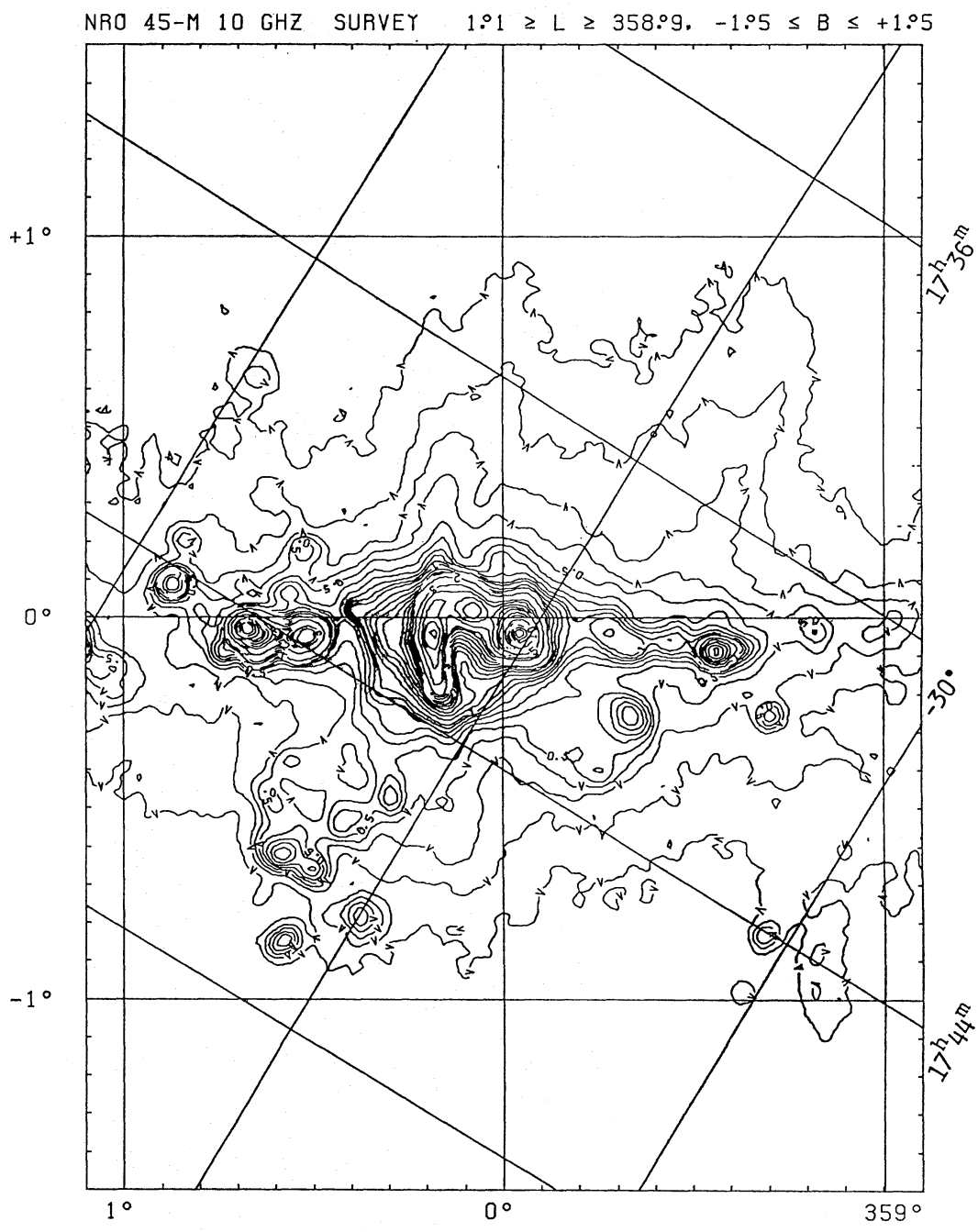


Fig. 31. See the caption of figure 3.

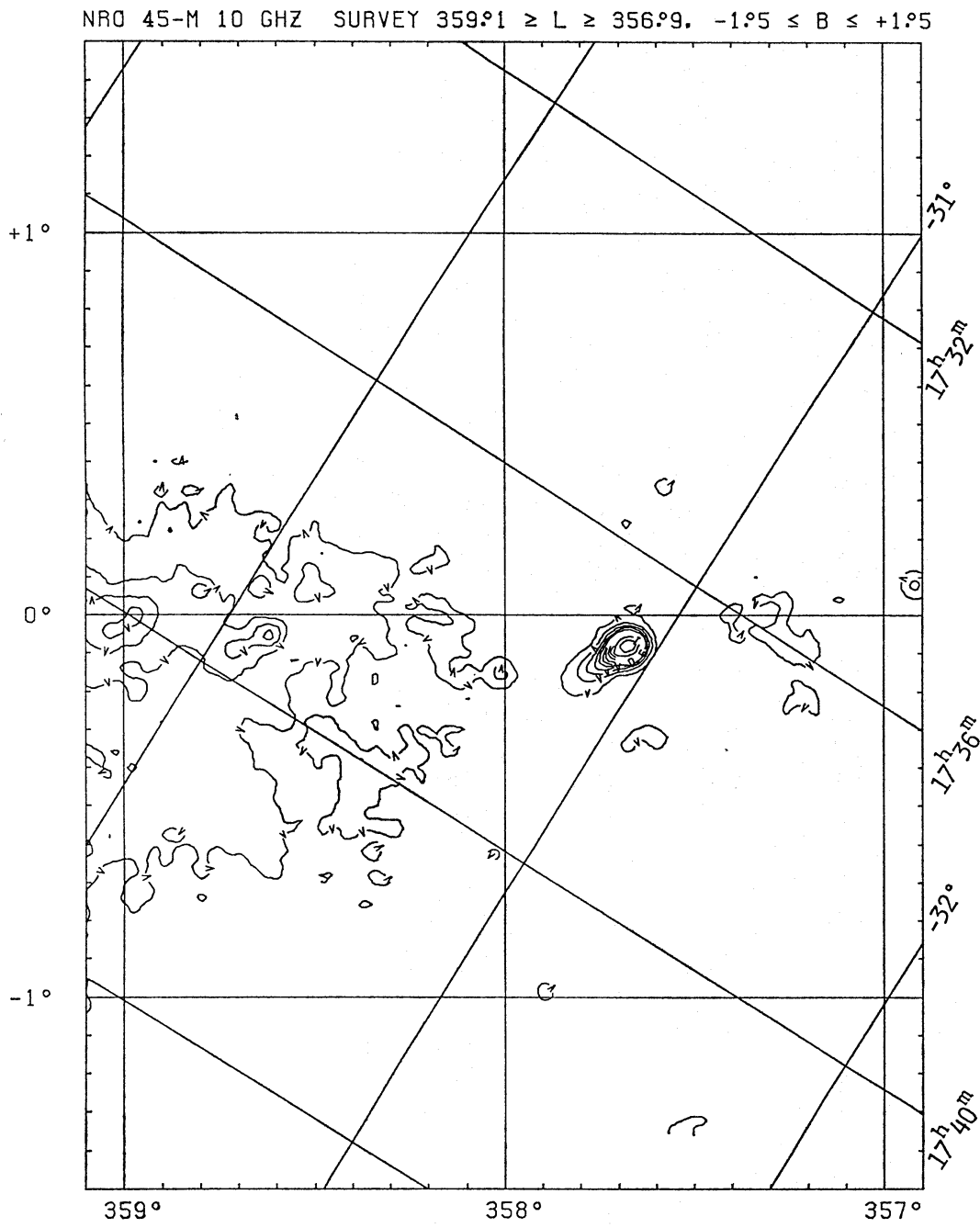


Fig. 32. See the caption of figure 3. The region $l \leq 358^{\circ}0$, $|b| \geq 1^{\circ}4$ have not been observed.

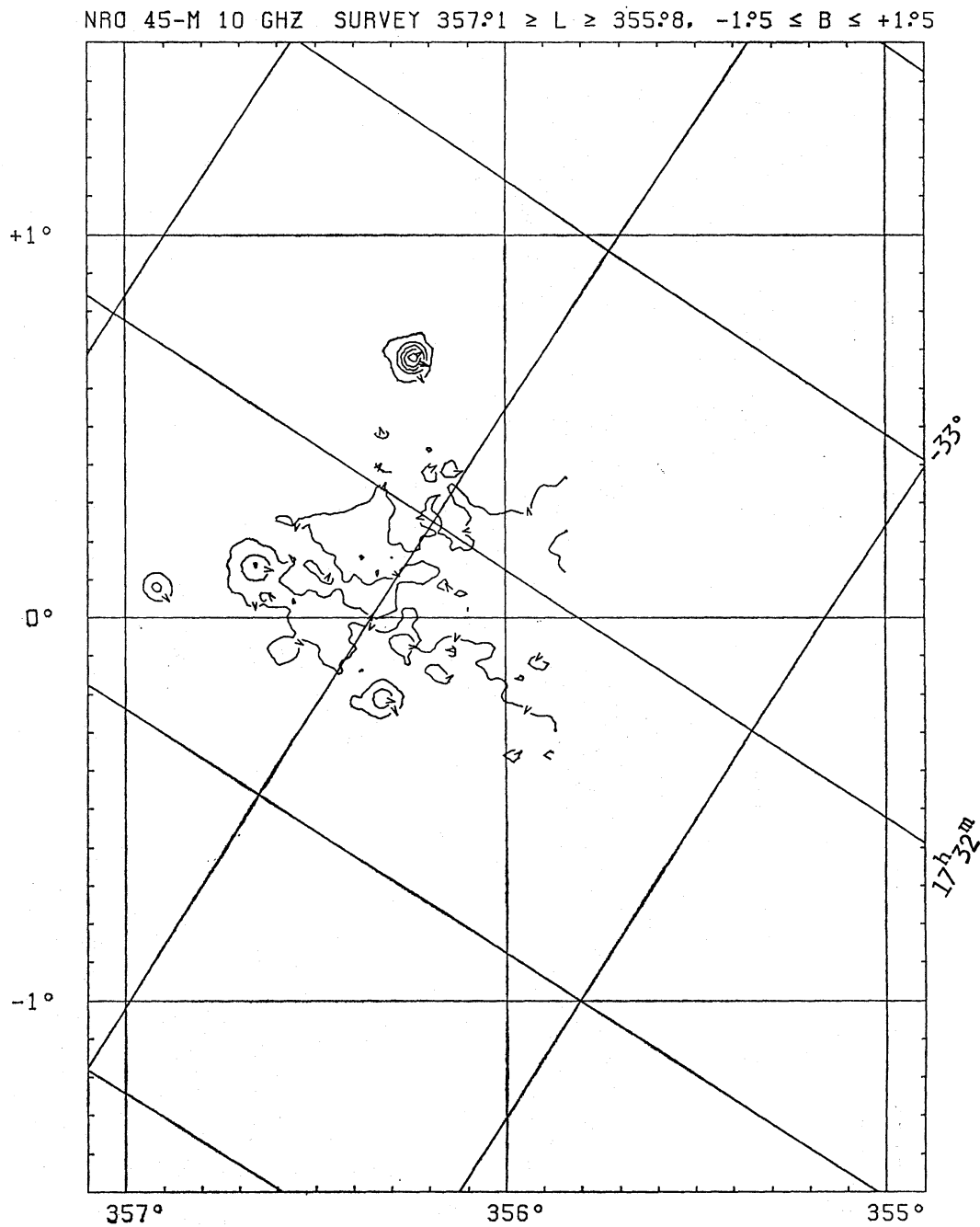


Fig. 33. See the caption of figure 3. The region $l \leq 355^{\circ}8$ and the region $|b| \geq 1^{\circ}4$ have not been observed.

Table 2. List of 144 small-diameter radio sources.

No.	<i>l</i> (degree)	<i>b</i> (degree)	R.A. (1950)	Decl.	Peak flux (Jy/beam)	Size	Flux (Jy)	Zero level K(T_B)	Remark
1 ...	356.244 0.000	0.678 0.000	17 ^h 30 ^m 26 ^s .8	-31°43'16"	1.46 0.02	3.37 0.06	1.84	0.071	
2 ...	356.324 0.001	-0.214 0.001	17 34 10.7	-32 08 24	0.61 0.02	3.28 0.12	0.73	0.077	
3 ...	356.917 0.001	0.079 0.001	17 34 31.6	-31 29 00	0.48 0.02	P		0.066	
4 ...	357.896 0.001	-0.986 0.001	17 41 11.7	-31 13 30	0.46 0.02	P		0.012	
5 ...	358.010 0.001	-0.155 0.001	17 38 11.3	-30 41 13	0.45 0.01	3.56 0.15	0.63	0.067	
6 ...	358.642 0.002	0.075 0.002	17 38 51.0	-30 01 47	0.44 0.04	P		0.142	
7 ...	358.802 0.002	0.059 0.002	17 39 18.4	-29 54 09	0.39 0.03	3.43 0.35	0.50	0.207	
8 ...	358.970 0.002	-0.728 0.002	17 42 48.1	-30 10 31	0.41 0.03	P		0.081	
9 ...	359.296 0.001	-0.258 0.001	17 41 44.8	-29 39 05	1.23 0.03	3.42 0.10	1.60	0.249	
10 ...	359.312 0.001	-0.832 0.001	17 44 2.3	-29 56 21	1.04 0.03	3.17 0.12	1.17	0.071	
11 ...	359.371 0.001	-0.984 0.001	17 44 46.8	-29 58 02	0.48 0.02	3.40 0.16	0.62	0.023	
12 ...	359.957 0.000	-0.043 0.000	17 42 30.5	-28 58 34	55.49 0.79	3.73 0.07	86.00	2.672	*
13 ...	0.295 0.002	-0.469 0.002	17 44 58.5	-28 54 40	1.17 0.11	3.15 0.35	1.30	0.442	
14 ...	0.524 0.002	0.179 0.002	17 43 0.2	-28 22 36	0.90 0.06	3.51 0.28	1.24	0.290	
15 ...	0.582 0.001	-0.852 0.001	17 47 9.1	-28 51 54	1.38 0.04	4.35 0.16	2.90	0.055	
16 ...	0.650 0.001	0.633 0.001	17 41 33.2	-28 01 53	0.54 0.01	4.38 0.14	1.14	0.082	
17 ...	0.873 0.001	0.087 0.001	17 44 11.4	-28 07 42	3.04 0.06	3.99 0.10	5.39	0.276	
18 ...	1.332 0.001	0.106 0.001	17 45 12.0	-27 43 33	0.76 0.03	4.04 0.17	1.38	0.181	
19 ...	5.198 0.001	-0.287 0.001	17 55 31.8	-24 36 26	0.58 0.02	3.74 0.13	0.89	0.021	
20 ...	5.489 0.001	-0.240 0.001	17 55 59.8	-24 19 56	1.07 0.03	3.72 0.11	1.65	0.087	

Table 2. (Continued)

No.	<i>l</i> (degree)	<i>b</i> (degree)	R.A. (1950)	Decl.	Peak flux (Jy/beam)	Size	Flux (Jy)	Zero level K(T_B)	Remark
21 ...	5.899 0.001	-0.404 0.001	17 ^h 57 ^m 31 ^s .4	-24°03'34"	8.58 0.28	3'.58 0.15	12.22	0.385	*
22 ...	6.101 0.001	-0.119 0.001	17 56 53.2	-23 44 31	1.10 0.04	4.39 0.20	2.35	0.240	
23 ...	6.396 0.002	-0.478 0.002	17 58 53.3	-23 39 58	0.69 0.03	4.41 0.27	1.49	0.274	
24 ...	6.561 0.001	-0.093 0.001	17 57 47.5	-23 19 51	2.55 0.05	3.31 0.08	3.12	0.401	
25 ...	7.477 0.000	0.067 0.000	17 59 10.7	-22 27 28	1.88 0.03	3.00 0.05	1.89	0.120	
26 ...	8.145 0.000	0.233 0.000	17 59 59.4	-21 47 45	4.56 0.05	3.35 0.05	5.70	0.092	
27 ...	8.677 0.001	-0.351 0.001	18 3 18.6	-21 37 22	1.50 0.04	P		0.189	
28 ...	8.867 0.002	-0.325 0.002	18 3 36.9	-21 26 40	0.61 0.04	P		0.184	
29 ...	9.630 0.001	0.202 0.001	18 3 15.6	-20 31 12	0.94 0.04	4.21 0.18	1.86	0.072	
30 ...	10.108 0.001	0.743 0.001	18 2 15.7	-19 50 15	0.61 0.02	P		0.044	
31 ...	10.168 0.001	-0.343 0.001	18 6 24.9	-20 19 08	26.53 0.63	3.28 0.10	31.67	0.584	*
32 ...	10.321 0.000	-0.145 0.000	18 5 59.7	-20 05 20	7.31 0.10	3.65 0.06	10.81	0.255	
33 ...	10.466 0.001	0.028 0.001	18 5 39.3	-19 52 39	1.05 0.03	3.43 0.12	1.37	0.166	
34 ...	10.630 0.001	-0.378 0.001	18 7 30.3	-19 56 00	5.19 0.08	3.67 0.07	7.78	0.157	
35 ...	10.704 0.002	0.041 0.002	18 6 6.0	-19 39 49	0.40 0.02	4.04 0.30	0.73	0.134	
36 ...	11.189 0.001	-0.346 0.001	18 8 32.5	-19 25 43	2.87 0.04	4.13 0.08	5.43	0.073	
37 ...	11.906 0.001	0.754 0.001	18 5 57.4	-18 16 00	1.06 0.03	4.32 0.17	2.21	0.037	
38 ...	11.946 0.001	-0.610 0.001	18 11 4.2	-18 53 40	1.67 0.04	P		0.048	
39 ...	11.951 0.001	-0.034 0.001	18 8 57.0	-18 36 40	1.44 0.06	3.40 0.17	1.86	0.152	
40 ...	12.213 0.000	-0.116 0.000	18 9 47.3	-18 25 19	1.65 0.02	3.75 0.07	2.59	0.180	

Table 2. (Continued)

No.	<i>l</i> (degree)	<i>b</i> (degree)	R.A. (1950)	Decl.	Peak flux (Jy/beam)	Size	Flux (Jy)	Zero level K(T_B)	Remark
41...	12.442 0.002	-0.041 0.002	18 ^h 9 ^m 58 ^s .9	-18°11'06"	0.48 0.03	3.41 0.23	0.62	0.177	
42...	12.814 0.001	-0.201 0.001	18 11 19.8	-17 56 13	27.09 0.51	3.07 0.07	28.40	0.649	*
43...	13.197 0.001	0.047 0.001	18 11 11.4	-17 28 54	2.56 0.05	3.49 0.08	3.46	0.237	
44...	13.219 0.001	-0.141 0.001	18 11 55.5	-17 33 13	1.09 0.02	P		0.175	
45...	13.388 0.002	0.077 0.002	18 11 28.1	-17 17 59	0.84 0.05	3.01 0.23	0.85	0.265	
46...	13.543 0.001	-0.179 0.001	18 12 43.2	-17 17 15	0.64 0.02	3.65 0.13	0.94	0.158	
47...	13.883 0.000	0.288 0.000	18 11 41.6	-16 45 52	3.28 0.04	3.21 0.05	3.76	0.130	
48...	14.459 0.001	-0.651 0.001	18 16 17.3	-16 42 35	0.84 0.02	4.19 0.14	1.64	0.176	
49...	15.162 0.002	-0.950 0.002	18 18 46.8	-16 14 02	1.13 0.08	3.85 0.35	1.87	0.565	
50...	16.744 0.001	0.081 0.001	18 18 8.1	-14 21 06	0.67 0.02	3.95 0.13	1.16	0.102	
51...	18.156 0.001	-0.283 0.001	18 22 12.4	-13 16 49	4.22 0.11	3.19 0.11	4.75	0.255	
52...	18.956 0.002	-0.014 0.002	18 22 46.9	-12 26 54	0.92 0.04	4.39 0.26	1.97	0.256	
53...	19.078 0.002	-0.267 0.002	18 23 56.1	-12 27 35	2.76 0.23	3.42 0.36	3.58	0.473	*
54...	19.492 0.001	0.146 0.001	18 23 14.3	-11 53 58	1.20 0.02	4.08 0.10	2.22	0.157	
55...	19.618 0.001	-0.229 0.001	18 24 49.9	-11 57 52	4.43 0.09	3.41 0.08	5.74	0.241	
56...	20.995 0.001	0.095 0.001	18 26 18.1	-10 35 50	0.99 0.02	3.13 0.09	1.08	0.101	
57...	21.357 0.001	-0.625 0.001	18 29 34.8	-10 36 49	0.89 0.02	3.01 0.09	0.90	0.082	
58...	21.521 0.000	-0.870 0.000	18 30 46.3	-10 34 58	5.66 0.07	3.13 0.04	6.15	0.054	
59...	21.877 0.001	0.017 0.001	18 28 15.6	-09 51 13	0.70 0.02	3.16 0.12	0.78	0.181	
60...	22.773 0.001	-0.477 0.001	18 31 43.6	-09 17 29	1.60 0.04	3.35 0.10	2.00	0.227	

Table 2. (Continued)

No.	<i>l</i> (degree)	<i>b</i> (degree)	R.A. (1950)	Decl.	Peak flux (Jy/beam)	Size	Flux (Jy)	Zero level K(T_b)	Remark
61 ...	23.270 0.002	-0.279 0.002	18 ^h 31 ^m 57 ^s .1	-08°45'34"	0.96 0.06	4.03 0.30	1.73	0.338	
62 ...	23.434 0.001	-0.198 0.001	18 31 58.1	-08 34 35	4.59 0.10	3.88 0.11	7.66	0.352	
63 ...	23.717 0.001	0.183 0.001	18 31 8.3	-08 08 54	1.58 0.05	3.13 0.12	1.72	0.260	
64 ...	23.880 0.001	-0.108 0.001	18 32 29.2	-08 08 25	0.98 0.02	3.06 0.08	1.01	0.198	
65 ...	23.966 0.000	0.163 0.000	18 31 40.6	-07 56 16	2.06 0.04	3.04 0.07	2.11	0.208	
66 ...	24.398 0.001	0.083 0.001	18 32 46.4	-07 35 31	1.14 0.04	3.98 0.18	2.00	0.296	
67 ...	24.477 0.000	0.502 0.000	18 31 25.6	-07 19 41	3.68 0.05	3.32 0.05	4.51	0.147	
68 ...	24.513 0.002	-0.027 0.002	18 33 22.9	-07 32 31	0.83 0.06	P		0.324	
69 ...	24.689 0.002	-0.142 0.002	18 34 7.4	-07 26 20	1.94 0.11	3.30 0.23	2.34	0.452	
70 ...	25.272 0.002	-0.308 0.002	18 35 48.3	-06 59 58	0.76 0.04	3.61 0.23	1.11	0.248	
71 ...	25.393 0.001	-0.169 0.001	18 35 32.0	-06 49 38	9.86 0.40	3.42 0.17	12.84	0.501	*
72 ...	25.394 0.002	-0.347 0.002	18 36 10.3	-06 54 32	0.69 0.05	3.45 0.31	0.91	0.257	
73 ...	25.406 0.001	0.039 0.001	18 34 49.0	-06 43 13	0.74 0.03	3.05 0.15	0.77	0.246	
74 ...	25.707 0.001	0.039 0.001	18 35 22.6	-06 27 09	1.18 0.05	3.77 0.20	1.86	0.280	
75 ...	26.546 0.000	0.421 0.000	18 35 34.7	-05 31 57	1.34 0.01	3.29 0.04	1.61	0.082	
76 ...	27.285 0.002	0.154 0.002	18 37 54.3	-05 00 03	0.82 0.04	3.91 0.24	1.40	0.204	
77 ...	27.388 0.001	-0.000 0.001	18 38 38.6	-04 58 52	0.72 0.03	3.60 0.18	1.04	0.181	
78 ...	27.500 0.001	0.192 0.001	18 38 9.9	-04 47 33	1.55 0.02	4.04 0.08	2.82	0.150	
79 ...	28.206 0.002	-0.043 0.002	18 40 18.7	-04 16 30	0.48 0.04	3.36 0.34	0.61	0.221	
80 ...	28.306 0.000	-0.373 0.000	18 41 40.3	-04 20 17	1.03 0.02	3.48 0.07	1.39	0.080	

Table 2. (Continued)

No.	<i>l</i> (degree)	<i>b</i> (degree)	R.A. (1950)	Decl.	Peak flux (Jy/beam)	Size	Flux (Jy)	Zero level K(T_B)	Remark
81...	28.607 0.001	-0.361 0.001	18 ^h 42 ^m 11. ^s 2	-04° 03' 56"	0.55 0.01	P		0.105	
82...	28.809 0.001	0.178 0.001	18 40 38.4	-03 38 19	1.54 0.07	P		0.280	
83...	28.830 0.001	-0.222 0.001	18 42 6.1	-03 48 13	0.75 0.02	4.06 0.11	1.38	0.144	
84...	28.992 0.002	-0.601 0.002	18 43 45.0	-03 50 04	0.52 0.03	3.85 0.28	0.86	0.096	
85...	29.706 0.001	-0.249 0.001	18 43 48.9	-03 02 21	1.21 0.03	3.25 0.10	1.42	0.156	
86...	30.409 0.002	-0.237 0.002	18 45 4.1	-02 24 35	1.04 0.10	P		0.384	
87...	30.701 0.001	-0.263 0.001	18 45 41.9	-02 09 42	1.42 0.06	3.78 0.18	2.26	0.337	
88...	30.777 0.001	-0.032 0.001	18 45 1.3	-01 59 18	25.63 0.58	4.42 0.13	55.68	0.872	*
89...	30.861 0.001	0.131 0.001	18 44 35.7	-01 50 17	1.18 0.06	3.13 0.21	1.29	0.446	
90...	30.970 0.003	0.598 0.003	18 43 8.3	-01 31 38	0.42 0.04	3.40 0.37	0.54	0.120	
91...	31.052 0.001	0.481 0.001	18 43 42.2	-01 30 28	0.78 0.03	3.73 0.16	1.20	0.136	
92...	31.064 0.002	0.078 0.002	18 45 9.4	-01 40 59	0.99 0.04	4.21 0.22	1.96	0.406	
93...	31.135 0.001	0.287 0.001	18 44 32.8	-01 31 24	0.59 0.02	3.65 0.17	0.87	0.174	
94...	31.280 0.002	0.067 0.002	18 45 35.7	-01 29 46	0.36 0.02	4.18 0.26	0.71	0.255	
95...	31.413 0.001	0.314 0.001	18 44 57.8	-01 15 54	0.94 0.02	P		0.120	
96...	31.616 0.001	0.338 0.001	18 45 15.0	-01 04 24	0.56 0.02	3.50 0.12	0.76	0.095	
97...	32.159 0.001	0.132 0.001	18 46 59.1	-00 41 08	0.69 0.04	P		0.127	
98...	32.265 0.002	1.174 0.002	18 43 28.7	-00 06 42	0.31 0.02	P		0.024	
99...	32.804 0.000	0.193 0.000	18 47 57.2	-00 05 08	4.09 0.03	P		0.114	
100...	33.505 0.001	0.199 0.001	18 49 13.4	+00 32 22	1.07 0.03	P		0.104	

Table 2. (Continued)

No.	<i>l</i> (degree)	<i>b</i> (degree)	R.A. (1950)	Decl.	Peak flux (Jy/beam)	Size	Flux (Jy)	Zero level K(T_B)	Remark
101 ...	33.817 0.001	-0.177 0.001	18 ^h 51 ^m 7 ^s .9	+00°38'39"	0.37 0.02	3.41 0.22	0.48	0.092	
102 ...	33.922 0.000	0.115 0.000	18 50 17.4	+00 52 18	1.04 0.02	P		0.114	
103 ...	34.131 0.001	0.469 0.001	18 49 24.9	+01 13 12	0.44 0.02	3.71 0.19	0.67	0.039	
104 ...	34.261 0.000	0.147 0.000	18 50 47.9	+01 11 13	11.72 0.11	3.03 0.04	11.97	0.181	
105 ...	35.046 0.001	-0.497 0.001	18 54 32.1	+01 35 16	0.93 0.02	3.32 0.09	1.14	0.040	
106 ...	36.553 0.002	0.008 0.002	18 55 31.1	+03 09 27	0.46 0.03	P		0.076	
107 ...	37.679 0.002	0.145 0.002	18 57 6.6	+04 13 11	0.80 0.04	3.99 0.26	1.40	0.187	
108 ...	37.772 0.001	-0.203 0.001	18 58 31.3	+04 08 33	2.46 0.11	3.10 0.17	2.63	0.239	
109 ...	37.883 0.001	-0.384 0.001	18 59 22.3	+04 09 24	4.62 0.14	P		0.221	
110 ...	39.266 0.001	-0.041 0.001	19 0 43.0	+05 32 30	1.40 0.06	3.36 0.17	1.75	0.110	
111 ...	41.129 0.001	-0.317 0.001	19 5 10.5	+07 03 54	2.58 0.15	3.04 0.22	2.65	0.193	
112 ...	41.240 0.002	0.364 0.002	19 2 57.0	+07 28 43	0.57 0.04	3.68 0.29	0.86	0.057	
113 ...	41.521 0.002	-0.142 0.002	19 5 17.1	+07 29 36	0.50 0.03	3.78 0.30	0.80	0.035	
114 ...	41.523 0.002	0.028 0.002	19 4 40.7	+07 34 25	0.71 0.03	4.35 0.22	1.49	0.038	
115 ...	42.108 0.001	-0.624 0.001	19 8 6.6	+07 47 19	1.69 0.05	3.34 0.12	2.09	0.064	
116 ...	42.109 0.002	-0.454 0.002	19 7 30.1	+07 52 05	0.54 0.05	P		0.064	
117 ...	42.437 0.001	-0.267 0.001	19 7 27.0	+08 14 45	1.00 0.05	P		0.092	
118 ...	43.169 0.001	0.002 0.001	19 7 52.1	+09 01 07	35.92 0.87	3.10 0.10	38.46	0.501	*
119 ...	43.184 0.001	-0.522 0.001	19 9 46.4	+08 47 17	0.84 0.05	P		0.095	
120 ...	43.263 0.001	-0.182 0.001	19 8 42.3	+09 00 57	6.28 0.15	3.70 0.11	9.54	0.117	

Table 2. (Continued)

No.	<i>l</i> (degree)	<i>b</i> (degree)	R.A. (1950)	Decl.	Peak flux (Jy/beam)	Size	Flux (Jy)	Zero level K(T_B)	Remark
121...	43.899 0.001	-0.784 0.001	19 ^h 12 ^m 3 ^s .8	+09°17'49"	0.96 0.06	P		0.018	
122...	44.269 0.002	0.106 0.002	19 9 34.5	+10 02 26	0.63 0.04	3.49 0.26	0.85	0.085	
123...	44.509 0.002	0.347 0.002	19 9 9.8	+10 21 55	0.66 0.06	P		0.037	
124...	45.130 0.000	0.146 0.000	19 11 4.0	+10 49 14	6.55 0.12	3.16 0.07	7.26	0.043	
125...	45.198 0.002	0.755 0.002	19 9 0.4	+11 09 55	0.39 0.04	P		0.023	
126...	45.394 0.002	-0.706 0.002	19 14 38.3	+10 39 13	0.48 0.03	3.37 0.24	0.61	0.060	
127...	45.458 0.001	0.072 0.001	19 11 57.8	+11 04 31	6.18 0.22	3.25 0.14	7.25	0.183	*
128...	45.840 0.002	-0.296 0.002	19 14 1.1	+11 14 25	0.54 0.05	3.24 0.34	0.63	0.051	
129...	46.499 0.001	-0.251 0.001	19 15 7.3	+11 50 35	1.82 0.06	4.28 0.19	3.70	0.064	
130...	48.600 0.001	0.040 0.001	19 18 8.5	+13 49 53	2.99 0.06	4.27 0.11	6.05	0.160	
131...	49.078 0.002	-0.382 0.002	19 20 36.6	+14 03 07	2.92 0.30	P		1.030	*
132...	49.208 0.001	-0.349 0.001	19 20 44.6	+14 10 56	9.50 0.25	3.28 0.11	11.34	0.590	*
133...	49.490 0.001	-0.373 0.001	19 21 22.9	+14 25 06	63.82 1.87	3.18 0.12	71.67	1.181	*
134...	49.708 0.002	-0.166 0.002	19 21 3.8	+14 42 34	0.40 0.02	3.84 0.24	0.65	0.061	
135...	50.235 0.001	0.337 0.001	19 20 16.2	+15 24 44	1.37 0.04	P		0.029	
136...	50.624 0.001	-0.019 0.001	19 22 20.4	+15 35 02	0.53 0.02	3.02 0.16	0.54	0.010	
137...	51.227 0.002	-1.395 0.002	19 28 33.0	+15 27 02	0.75 0.05	3.03 0.25	0.77	0.018	
138...	51.367 0.001	0.007 0.001	19 23 43.4	+16 14 56	1.90 0.07	3.37 0.16	2.41	0.164	
139...	51.753 0.002	0.799 0.002	19 21 35.3	+16 58 01	0.48 0.04	3.46 0.33	0.63	0.034	
140...	52.085 0.002	1.050 0.002	19 21 19.6	+17 22 40	0.49 0.04	P		0.019	

Table 2. (Continued)

No.	<i>l</i> (degree)	<i>b</i> (degree)	R.A. (1950)	Decl.	Peak flux (Jy/beam)	Size	Flux (Jy)	Zero level K(T_B)	Remark
141 ...	52.229 0.002	0.736 0.002	19 ^h 22 ^m 46 ^s .4	+17°21'18"	0.78 0.04	4'.50 0.26	1.76	0.024	
142 ...	52.756 0.002	0.339 0.002	19 25 17.6	+17 37 35	0.46 0.03	3.42 0.23	0.60	0.025	
143 ...	53.186 0.001	0.164 0.001	19 26 48.5	+17 55 10	1.48 0.04	3.39 0.12	1.89	0.054	
144 ...	54.095 0.001	-0.063 0.001	19 29 29.9	+18 36 17	1.14 0.03	4.44 0.12	2.49	0.063	

The root mean square of the residual values after the fitting is less than 15% of the peak intensity.

The positions, peak flux densities, and sizes of the sources were derived by a Gaussian fitting procedure. A single, round-shaped, two-dimensional Gaussian surface superposed on an inclined plane was applied to a properly selected small area of 7'.6 square around each source.

The column entry to table 2 is explained below:

Column 1: Serial number.

Columns 2 and 3: Galactic longitude and latitude.

Columns 4 and 5: Right ascension and declination for epoch 1950.0.

Column 6: Peak flux density in Jy/3'.0 beam.

Column 7: Apparent diameter at the full width of the half maximum (HPBW=3'.0). Designation P indicates a pointlike source with size smaller than 3'.0.

Column 8: Integrated flux density in units of jansky using the parameters of columns 6 and 7.

Column 9: The base level derived from the fitting in kelvins (T_B). Note that some sources in complex regions may not take proper levels because of the complicated background emission.

Column 10: If an asterisk is marked on the column, the root mean square of the residual values after the fitting is greater than 0.3 Jy/3'.0 beam. In this case the shape of the source may be deviated from the Gaussian distribution and its parameters may be invalid.

Columns 2, 3, 6, and 7 give also the mean errors of each entry on the second line.

The authors acknowledge K. Akabane of NRO for his continuous encouragement and his support during all stages of this project. They also acknowledge the staff of NRO for help in the observations. Especially, they would like to thank K. Miyazawa of NRO for maintaining the 10-GHz receiver. They would like to thank E. Fürst, W. Reich, and P. Reich of Max-Planck-Institut für Radioastronomie for the help in developing reduction software and S. Kobayashi of the Advanced Information Design Co. for developing the display system at NRO. They also thank H. Tabara and T.

Kato of Utsunomiya University for their advice about intensity calibration and encouragement. They would like to thank the referees for improving the English expression and useful advice.

References

- Altenhoff, W. J., Downes, D., Goad, L., Maxwell, A., and Rinehart, R. 1970, *Astron. Astrophys. Suppl.*, **1**, 319.
- Altenhoff, W. J., Downes, D., Pauls, T., and Schraml, J. 1979, *Astron. Astrophys. Suppl.*, **35**, 23.
- Andrew, B. H., MacLeod, J. M., and Feldman, P. A. 1981, *Astron. Astrophys.*, **99**, 36.
- Day, G. A., Caswell, J. L., and Cooke, D. J. 1972, *Australian J. Phys. Astrophys. Suppl.*, No. 25.
- Haslam, C. G. T. 1974, *Astron. Astrophys. Suppl.*, **15**, 333.
- Haynes, R. F., Caswell, J. L., and Simons, L. W. J. 1978, *Australian J. Phys. Astrophys. Suppl.*, No. 45.
- Hirabayashi, H. 1974, *Publ. Astron. Soc. Japan*, **26**, 263.
- Reich, W., Fürst, E., Steffen, P., Reif, K., and Haslam, C. G. T. 1984, *Astron. Astrophys. Suppl.*, **58**, 197.
- Sofue, Y., Hirabayashi, H., Akabane, K., Inoue, M., Handa, T., and Nakai, N. 1984, *Publ. Astron. Soc. Japan*, **36**, 287.
- Sofue, Y., and Reich, W. 1979, *Astron. Astrophys. Suppl.*, **38**, 251.